Kääb et al. (2012): Contrasting patters of early twenty-first-century glacier mass change in the Himalayas.
Nature. 23 August 2012. Vol 488, issue 7412, pages 495-498, doi:10.1038/nature11324.
Final Manuscript

Contrasting patterns of early twenty-first-century glacier mass change in the Himalayas

Andreas Kääb[1], Etienne Berthier[2], Christopher Nuth[1], Julie Gardelle[3] & Yves Arnaud[4]

[1]Department of Geosciences, University of Oslo, PO Box 1047, Blindern, 0316 Oslo, Norway.

[2]CNRS, Université de Toulouse, LEGOS, 14 avenue Ed. Belin, Toulouse 31400, France.

[3]CNRS- Université Grenoble 1, LGGE, 54 rue Molière, BP 96, 38402 Saint Martin d'Hères Cedex, France.

[4]IRD- Université Grenoble 1, LTHE/LGGE, 54 rue Molière, BP 96, 38402 Saint Martin d'Hères Cedex, France.

Glaciers are among the best indicators of terrestrial climate variability, contribute importantly to water resources in many mountainous regions[1,2] and are a major contributor to global sea level rise[3,4]. In the Hindu Kush–Karakoram–Himalaya region (HKKH), a paucity of appropriate glacier data has prevented a comprehensive assessment of current regional mass balance[5]. There are, however, indirect evidences of a complex pattern of glacial responses[5–8] in reaction to heterogeneous climate change signals[9]. Here we use satellite laser altimetry and a global elevation model to show widespread glacier wastage in the eastern, central and south-western parts of the HKKH during 2003–08. Maximal regional thinning rates were 0.66 ± 0.09 metres per year in the Jammu–Kashmir region. Conversely, in the Karakoram, glaciers thinned only slightly by a few centimetres per year. Contrary to expectations, regionally averaged thinning rates under debris-mantled ice were similar to those of clean ice despite insulation by debris covers. The 2003–08 specific mass balance for our entire HKKH study region was −0.21 ± 0.05 m yr^{-1} water equivalent, significantly less negative than the estimated global average for glaciers and ice caps[4,10]. This difference is mainly an effect of the balanced glacier mass budget in the Karakoram. The HKKH sea level contribution amounts to 1% of the present-day sea level rise[11]. Our 2003–08 mass budget of −12.8 ± 3.5 gigatonnes (Gt) per year is more negative than recent satellite-gravimetry-based estimates of −5 ± 3 Gt yr^{-1} over 2003–10 (ref. 12). For the mountain catchments of

the Indus and Ganges basins[13], the glacier imbalance contributed about 3.5 % and about 2.0%, respectively, to the annual average river discharge[13], and up to 10% for the Upper Indus basin[14].

The HKKH is an ensemble of mountain ranges stretching east to west over 2,000 km, containing around 60,000 km^2 of glaciers, glacierets and perennial surface ice in varying climatic regimes. In the east, glaciers receive most accumulation during summer from the Indian monsoon, whereas in the west they accumulate snow mostly in winter through westerly atmospheric circulations[9,13,15]. In addition, a strong northward decrease in precipitation is caused by the extreme topography. Therefore, variability in observed glacier changes within the region is large[5–8,16–19], and quantifying the current glacier mass change and its impacts on sea-level rise, water resources and natural hazards is hampered by a lack of sufficiently distributed and accurate data. The annual glacier mass balances of a few small and mainly debris-free glaciers[18,20] are unlikely to be representative of the entire region.

In this study, we provide glacier thickness changes and estimated mass changes over the HKKH, specifically the Indus and Ganges river basins and their surroundings (Fig. 1). This is achieved by combining two elevation data sets, the sparse laser measurements from the Ice, Cloud and land Elevation Satellite (ICESat) over 2003–09 and the Digital Elevation Model (DEM) from the Shuttle Radar Topography Mission (SRTM) of February 2000. Standard ICESat analysis[21] is not applicable in the HKKH owing to large cross-track separation and topographic roughness between repeat tracks. Unknown and spatially variable penetration of the SRTM 5.6-cm radar waves (C-band) into snow and ice[22,23] also complicates the direct extraction of glacier thickness changes from the differences between the SRTM and ICESat elevations.

However, the SRTM DEM ensures that the repeat ICESat analysis samples consistent slopes and similar hypsometry over time so that temporal trends in elevation difference can be estimated through the entire ICESat acquisition series (Figs 1 and 2). The SRTM DEM is subtracted from all footprint elevations. The digital numbers of multispectral Landsat images of around the year 2000, selected with minimum snow cover, are extracted for each ICESat footprint for initial classification into five categories (glacier clean ice, glacier debris cover, glacier firn and snow, open water and

off-glacier) and then manually edited. The last ICESat campaign (2F) before sensor failure, and the June campaigns (2C, 3C, 3F) are excluded (Methods, Supplementary Information).

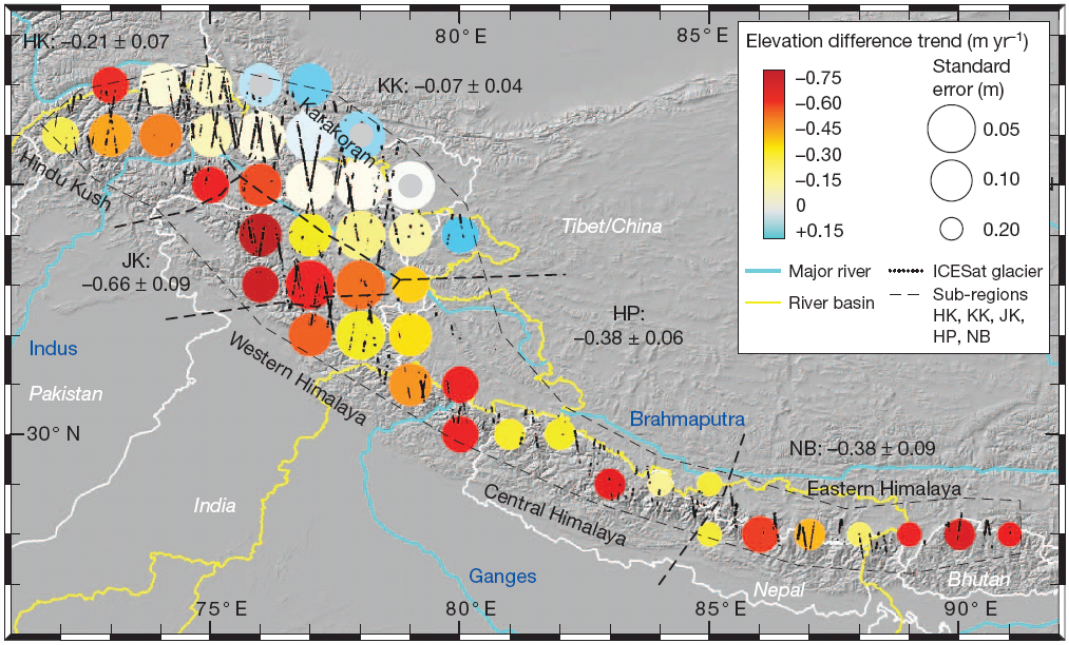

Figure 1 Study region and trends of elevation differences between ICESat and SRTM over 2003–08. Data are shown on a 1° grid with overlapping rectangular geographic averaging cells of 2° × 2°. Trends are based on autumn ICESat acquisitions. The mean trends for each subregion are given in metres per year. Only ICESat footprints over glaciers are indicated. Trends for all cells (coloured data circles) are statistically significant except for three cells in the Karakoram that are indicated with grey centres. Errors are one standard error (1 s.e.).

On glaciers, elevation difference trends derived over 2°× 2°-sized geographic cells depict pronounced regional variations (Fig. 1) and suggest, together with climatological and glaciological patterns, five major sub-regions for further analysis: the Hindu-Kush south of the Wakhan Corridor (HK), the Karakoram (KK), Jammu–Kashmir (JK), Himachal Pradesh, Uttarakhand and West Nepal (HP), and East Nepal and Bhutan (NB). On the basis of the autumn ICESat data only (2003–08), HKKH glaciers thinned on average, –0.26 ± 0.06 m yr^{-1}, and in all subregions with significant spatial differences (Figs 1 and 2; Table 1). (Error levels correspond to one standard error; Supplementary Information). Thickening is found only in the northern and eastern parts of KK (northeast of the Indus basin): +0.14 ± 0.06 m yr^{-1}). Disregarding

ice/firn/snow footprints that cannot clearly be assigned to a glacier has no significant effect on the trends in HK, KK and JK but leads to 25% and 50% more-negative trends in HP and NB, respectively (Supplementary Information).

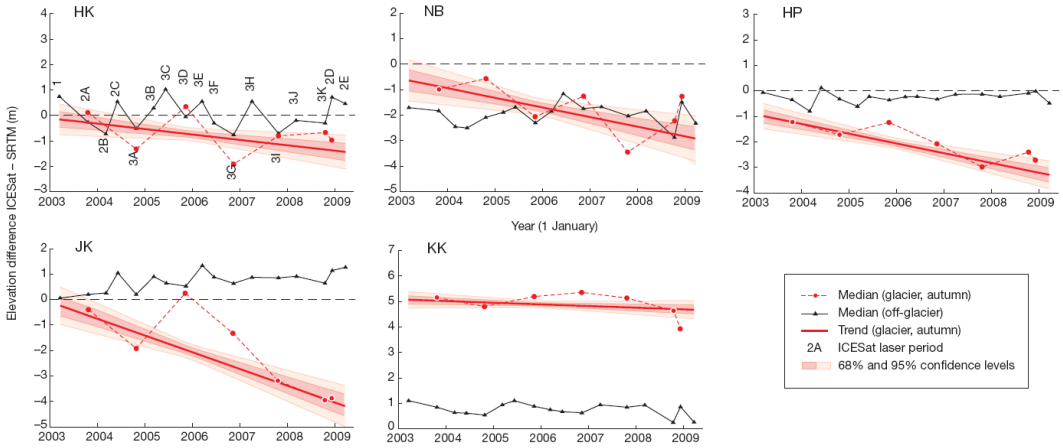

Figure 2 Median elevation differences between ICESat and SRTM for ICESat laser periods and glacier elevation difference trends. Data are given for the five sub-regions defined in Fig. 1. For off-glacier terrain (black triangles and curves) all medians are shown; for glaciers only autumn laser altimetry periods (red dots and dashed curves; compare Supplementary Fig. 2) are shown. Autumn trends (red bold lines) are fitted through all individual elevation differences using a robust fitting method, not through the laser altimetry period median elevation differences, creating small offsets between the trends shown and a virtual regression through the laser period medians. The 68% and 95% confidence levels (shaded medium red and light red) represent solely the statistical error of the trend fitting.

Comparing the autumn glacier trends, which represent annual glacier mass balances, to trends from winter ICESat data (Supplementary Information) suggests an increasing mass turnover in KK and JK. The similarity between autumn and winter trends in HP and NB is consistent with glaciers in the east being of the summer-accumulation type[15]. For off-glacier terrain, secular trends are statistically indistinguishable from zero (Table 1). Off-glacier seasonal cycles are minimal (largest for HK) yet roughly congruent with glacier seasonality (Fig. 2).

C-band SRTM elevations are influenced by the varying penetration of the radar wave into ice, firn and snow[22,23]. Consequently, extrapolation of ICESat-derived glacier elevation trends (Fig. 2) back to the SRTM acquisition date of February 2000 reveals first-order C-band penetration estimates of several metres, largest for firn/snow and

smallest for debris-covered ice, and largest for KK and smallest for HP and NB (Supplementary Table 2).

For the entire HKKH, our elevation trends on clean and debris-covered ice show no significant difference (Table 1). To avoid bias related to differences in the geographic and topographic distributions between clean and debris-covered ice, this comparison is based upon pairs of footprints sharing similar location, elevation, slope and aspect. For KK, JK, HP and NB, thinning on debris-covered ice is not statistically different from, and for HK exceeds, thinning on clean ice[17,19,24] despite the widely assumed insulating effect of debris[25]. In KK, though, the sparse ICESat tracks might not sample the high variability of elevation changes, in particular of the glacier tongues[19], in a regionally representative way. Glacier elevation changes at a specific location are the combined effect of surface mass balance and ice flux budget. Given that our pairs of neighbouring footprints (mean distance between them is approximately 1 km) typically occur on the same glacier, differences in ice flux budget within a pair are expected to be small. Thus, we assume that the comparison between clean and debris-covered ice elevation trends at least partly reflects differences in ablation rates of the two. The similar thinning rates between both glacier cover types are presumably caused by thermokarst processes on debris-covered tongues that are dynamically inactive[6,17,26,27]. Our findings suggest that the well-proved insulating effect of debris layers with thicknesses exceeding a few centimetres[28] acts on local scales of intact covers, but not in general on the spatial scale of entire glacier tongues. The substantial ice thickness loss over debris-covered ice allows continued, and possibly enhanced, evolution of supraglacial and moraine lakes, and associated outburst hazards[7,29].

Scaling up of ICESat footprint classes indicates a total perennial surface ice area of around 60,000 km^2 (Table 1, Supplementary Information). Using a glacier mask based on a ratio between visible and short-wave infrared Landsat bands and glacier inventories available for the HKKH, the SRTM glacier hypsometry verifies the spatial and hypsometric representativeness of the ICESat footprint classification and distribution for all HKKH glaciers (Supplementary Fig. 3), so elevation difference trends can be applied to the total ice-covered area. A first density scenario (a) assumes all glacier thickness changes are loss and gain of ice (900 kg m^{-3}), a second density scenario (b) assumes 900 kg m^{-3} for thickness changes over ice and 600 kg m^{-3} for

changes over firn and snow (Table 1, Supplementary Information). Our final mass budget estimate is the average of the two scenarios (ab), resulting in a mass change of -12.8 ± 3.5 gigatonnes per year (Gt yr^{-1}) and a sea level rise contribution of 0.035 ± 0.009 mm yr^{-1} for HKKH glaciers, which is 3% to 4% of the total contribution from global glaciers and ice caps[3,4].

The specific mass balances measured on HKKH glaciers over 2003–08 are less negative than various estimates of the global average for glaciers and ice caps outside Greenland and Antarctica of around –0.75 m yr^{-1} water equivalent (WE)[4,10] based on in-situ mass-balance measurements. Our 2003–08 HKKH mass budget of -12.8 ± 3.5 Gt yr^{-1} is, however, considerably more negative than a recent estimate of -5 ± 3 Gt yr^{-1} based on satellite gravimetry (GRACE) over 2003–10 (ref. 12; their original uncertainty at 2-sigma level was converted to 1-sigma level; see Supplementary Information for full multi-study comparisons).

The annual average 2003–08 glacier imbalances for the Indus (about 1,150,000 km^2) and Ganges (~1,030,000 km^2) basins amount to approximately 300 ± 53 m^3 s^{-1} discharge equivalent (mass imbalance units of Gt yr^{-1} converted to m^3 s^{-1}) for the Indus basin and approximately 185 ± 45 m^3 s^{-1} for the Ganges basin, respectively, neglecting any processes other than direct river runoff. The actual contribution of glacier imbalance to total discharge depends on the distance from glaciers and the seasonality of the glacier imbalance[1], which is, however, not directly accessible from our ICESat measurements. As an annual average for the combined outlets of the mountain catchments within the Indus and Ganges river basins defined by ref. 13 (the Indus about 320,000 km^2, and the Ganges about 182,000 km^2; Supplementary Fig. 1) and neglecting any water loss due to evaporation or groundwater storage, our glacier imbalances amount to about 3.5% and about 2.0% of the total modelled discharges[13] for the Indus and Ganges mountain catchments, respectively. For the outlet of the Upper Indus basin (~200,000 km^2, Supplementary Fig. 1) at the Tarbela dam[14] the annual average glacier imbalance, about 231 ± 46 m^3 s^{-1}, amounts to about 10% of the modelled and measured annual river discharge[14], and explains most of the approximately 300 m^3 s^{-1} discrepancy between total annual precipitation (311 mm yr^{-1} or around 1,980 m^3 s^{-1}) and observed annual stream flow (around 2,290 m^3 s^{-1}) (ref.

14). The increase of precipitation with altitude (unaccounted for in the mean basin precipitation estimate[14]) may also have contributed to this discrepancy[30].

The glacier thickness changes presented here underpin the first spatially resolved mass budget over the entire HKKH, and in turn the first quantitative observational assessment of the contribution of glacier imbalance to river runoff, to our knowledge. That debris-covered ice thins at a rate similar to that of exposed ice shows that the role of debris mantles in glacier mass balance must be reassessed. In particular, in regions of highly discontinuous glacier coverage, we suggest that satellite gravimetry will be very useful to better detect large-scale sub-surface mass changes such as from hydrology or tectonics, or to better quantify errors in the corrections of these, respectively, by relying on glacier mass changes from studies such as ours. Our results will thus enable improved estimates of groundwater depletion in northern India[31] , which has thus far been difficult to discriminate from glacier loss in satellite gravity observations[12].

Table 1 | Glacier elevation difference trends and mass balances 2003–09

	Hindu Kush (HK)	Karakoram (KK)	Jammu Kashmir (JK)	Himachal Pradesh, Uttarakhand and West Nepal (HP)	East Nepal and Bhutan (NB)	Sum (first 3 rows) or area-weighted mean (HKKH)
Glacier area (km^2)	9,350	21,750	4,900	14,550	9,550	60,100
Number of ICESat glacier footprints (Oct–Nov)	6,300	18,050	4,200	9,850	5,650	44,050
Number of ICESat glacier footprints (Feb–Mar)	4,600	12,050	2,750	6,800	5,050	31,250
Clean ice/debris-covered ice/AAR around year 2000 (as percentage of glacier area)	54 / 16 / 30	44 / 9 / 47	57 / 14 / 29	51 / 14 / 35	38 / 15 / 47	47 / 13 / 40
Elevation difference trends ($m\,yr^{-1} \pm 1$ s.e.)						
Off-glacier	$+0.01 \pm 0.05$	-0.02 ± 0.02	$+0.02 \pm 0.05$	$+0.01 \pm 0.02$	-0.02 ± 0.04	0.0 ± 0.03
Glaciers (Oct–Nov 2003–08)	-0.21 ± 0.07	-0.07 ± 0.04	-0.66 ± 0.09	-0.38 ± 0.06	-0.38 ± 0.09	-0.26 ± 0.06
Glaciers (Feb–Mar 2003–09)	-0.48 ± 0.07	$+0.41 \pm 0.04$	-0.26 ± 0.09	-0.38 ± 0.06	-0.38 ± 0.09	-0.10 ± 0.06
Clean ice	-0.21 ± 0.32	-0.54 ± 0.25	-1.28 ± 0.54	-1.20 ± 0.33	-2.30 ± 0.53	-0.78 ± 0.16
Debris−covered ice	-1.54 ± 0.31	-0.04 ± 0.26	-1.05 ± 0.44	-1.02 ± 0.29	-1.53 ± 0.43	-0.76 ± 0.16
Mass balance						
Density scenario a ($m\,yr^{-1}$ WE ± 1 s.e.)	-0.19 ± 0.06	-0.06 ± 0.04	-0.59 ± 0.08	-0.34 ± 0.05	-0.34 ± 0.08	-0.23 ± 0.05
Density scenario a ($Gt\,yr^{-1} \pm 1$ s.e.)	-1.8 ± 0.6	-1.3 ± 0.9	-2.9 ± 0.5	-5.0 ± 0.9	-3.3 ± 0.9	-14.3 ± 3.5
Density scenario b ($m\,yr^{-1}$ WE ± 1 s.e.)	-0.20 ± 0.05	0.0 ± 0.03	-0.51 ± 0.06	-0.30 ± 0.04	-0.26 ± 0.07	-0.19 ± 0.04
Density scenario b ($Gt\,yr^{-1} \pm 1$ s.e.)	-1.8 ± 0.5	0.0 ± 0.8	-2.5 ± 0.4	-4.4 ± 0.8	-2.5 ± 0.7	-11.2 ± 3.1
Density scenario ab ($m\,yr^{-1}$ WE ± 1 s.e.)	-0.20 ± 0.06	-0.03 ± 0.04	-0.55 ± 0.08	-0.32 ± 0.06	-0.30 ± 0.09	-0.21 ± 0.05
Density scenario ab ($Gt\,yr^{-1} \pm 1$ s.e.)	-1.8 ± 0.6	-0.6 ± 0.9	-2.7 ± 0.5	-4.7 ± 1.0	-2.9 ± 0.9	-12.8 ± 3.5
Density scenario ab ($mm\,yr^{-1}$ SLE ± 1 s.e.)	-0.005 ± 0.002	-0.001 ± 0.002	-0.008 ± 0.001	-0.013 ± 0.003	-0.008 ± 0.003	-0.035 ± 0.009

All analyses refer to the perennial surface ice features such as glaciers, glacierets and perennial ice patches. Footprints over SRTM voids and from laser period 2F are discarded. Errors given (one standard error, s.e.) are the root of sum of squares (RSS) of the standard error of fits, the off-glacier trend, and a simulated effect of elevation variations within a season. Elevation difference trends for clean and debris-covered ice were computed for pairs of neighbouring footprints on clean and debris-covered ice. The density assumption scenarios are: a, 900 $kg\,m^{-3}$; b, 900 $kg\,m^{-3}$ for ice and 600 $kg\,m^{-3}$ for firn and snow footprints; ab is the mean of scenarios a and b. The error of scenario ab is a combined error (RSS) including the trend error and the standard deviation of the mean of scenarios a and b. For the total mass changes ($Gt\,yr^{-1}$) and sea level equivalent (SLE), the errors also include (RSS) a 10% uncertainty for the glacier areas. AAR, accumulation area ratio (here the ratio between snow and firn areas to total glacier area); WE, water equivalent.

METHODS SUMMARY

Cloud-free 30-m resolution Landsat TM or ETM Landsat Thematic Mapper (TM) and Enhanced Thematic Mapper (ETM) scenes from around the year 2000 with minimal snow cover were obtained from the United States Geological Survey as a topographically corrected version (L1T; http://glovis.usgs.gov; Supplementary Table 1). A band ratio denotes snow/firn/clean ice areas (Supplementary Data). All ICESat footprint elevations during 2003–09 (about 70 m footprint diameter and 170 m along-track spacing), obtained from the National Snow and Ice Data Center (http://nsidc.org/data/icesat/index.html; release 531), within a 10-km buffer around the snow/firn/clean-ice mask are compared to the ~90-m gridded SRTM DEM for February 2000 (void-filled version 4 from the Consultative Group on International Agricultural Research; http://srtm.csi.cgiar.org/) through bilinear interpolation of the estimated footprint centre. ICESat points within the SRTM void mask are disregarded. SRTM geoid elevations are converted from the Earth Gravity Model (EGM) 1996 to EGM2008, which is used for ICESat release 531. The SRTM DEM is co-registered with the 17 ICESat campaigns. Landsat band ratios for snow/firn/clean ice and snow/firn were computed at ICESat footprint locations. Footprints over debris-covered glacier sections are initially labelled using glacier outlines, where available (http://glims.colorado.edu/glacierdata/, http://glims.org/RGI/randolph.html). The footprint classifications were superimposed over the Landsat mosaic and edited manually to clean ice, snow/firn, debris-covered ice and off-glacier classes, and to introduce an additional water class (Supplementary Data). Elevation trends were derived using a robust linear regression through all ICESat-SRTM elevation differences. Various tests (Supplementary Information) showed that these trends are not very sensitive to the type of ICESat waveform fitting, the spatial elevation sampling and the timing of ICESat acquisitions. Interestingly, an even lower spatial sampling than the ICESat acquisition programme would produce significant results. Histogram adjustments were required to compare off- and on-glacier trends due to significant biases from saturation of ICESat waveforms on steep slopes, mainly off-glacier. Glacier thickness changes were converted to mass changes using two density scenarios. More details about the data and methods can be found in the Supplementary Information.

Received 13 April; accepted 12 June 2012; doi:10.1038/nature11324.

References

1 Kaser, G., Grosshauser, M. & Marzeion, B. Contribution potential of glaciers to water availability in different climate regimes. *P. Natl. Acad. Sci. USA* **107**, 20223-20227 (2010).

2 Immerzeel, W. W., van Beek, L. P. H. & Bierkens, M. F. P. Climate change will affect the Asian water towers. *Science* **328**, 1382-1385 (2010).

3 Church, J. A. *et al.* Revisiting the Earth's sea-level and energy budgets from 1961 to 2008. *Geophys. Res. Lett.* **38**, L18601 (2011).

4 Cogley, J. G. Geodetic and direct mass-balance measurements: comparison and joint analysis. *Ann. Glaciol.* **50**, 96-100 (2009).

5 Bolch, T. *et al.* The state and fate of Himalayan glaciers. *Science* **336**, 310-314 (2012).

6 Scherler, D., Bookhagen, B. & Strecker, M. R. Spatially variable response of Himalayan glaciers to climate change affected by debris cover. *Nature Geosc.* **4**, 156-159 (2011).

7 Gardelle, J., Arnaud, Y. & Berthier, E. Contrasted evolution of glacial lakes along the Hindu Kush Himalaya mountain range between 1990 and 2009. *Global Planet. Change* **75**, 47-55 (2011).

8 Hewitt, K. Glacier change, concentration, and elevation effects in the Karakoram Himalaya, Upper Indus Basin. *Mt. Res. Dev.* **31**, 188-200 (2011).

9 Fowler, H. J. & Archer, D. R. Conflicting signals of climatic change in the Upper Indus basin. *J. Climate* **19**, 4276-4293 (2006).

10 WGMS. *World Glacier Monitoring Service, www.wgms.ch*, (2012).

11 Cazenave, A. *et al.* Sea level budget over 2003-2008: A reevaluation from GRACE space gravimetry, satellite altimetry and Argo. *Glob. Planet. Change* **65**, 83-88 (2009).

12 Jacob, T., Wahr, J., Pfeffer, W. T. & Swenson, S. Recent contributions of glaciers and ice caps to sea level rise. *Nature* **482**, 514-518 (2012).

13 Bookhagen, B. & Burbank, D. W. Toward a complete Himalayan hydrological budget: spatiotemporal distribution of snowmelt and rainfall and their impact on river discharge. *J. Geophys. Res.* **115**, F03019 (2010).

14 Immerzeel, W. W., Droogers, P., de Jong, S. M. & Bierkens, M. F. P. Large-scale monitoring of snow cover and runoff simulation in Himalayan river basins using remote sensing. *Remote Sens. Environ.* **113**, 40-49 (2009).

15 Fujita, K. Effect of precipitation seasonality on climatic sensitivity of glacier mass balance. *Earth Planet. Sc. Lett.* **276**, 14-19 (2008).

16 Berthier, E. *et al.* Remote sensing estimates of glacier mass balances in the Himachal Pradesh (Western Himalaya, India). *Rem. Sens. Env.* **108**, 327-338 (2007).

17 Bolch, T., Pieczonka, T. & Benn, D. Multi-decadal mass loss of glaciers in the Everest area (Nepal Himalaya) derived from stereo imagery. *Cryosphere*, 349-358 (2011).

18 Fujita, K. & Nuimura, T. Spatially heterogeneous wastage of Himalayan glaciers. *P. Natl. Acad. Sci. USA* **108**, 14011-14014 (2011).

19 Gardelle, J., Berthier, E. & Arnaud, Y. Slight mass gain of Karakoram glaciers in the early 21st century. *Nature Geosci.* **5**, 322-325 (2012).

20 Azam, M. F. *et al.* From balance to imbalance: a shift in the dynamic behaviour of Chhota Shigri Glacier (Western Himalaya, India). *J. Glaciol.* **58**, 315-324 (2012).

21 Moholdt, G., Nuth, C., Hagen, J. O. & Kohler, J. Recent elevation changes of Svalbard glaciers derived from ICESat laser altimetry. *Remote Sens. Environ.* **114**, 2756-2767 (2010).

22 Rignot, E., Echelmeyer, K. & Krabill, W. Penetration depth of interferometric synthetic-aperture radar signals in snow and ice. *Geophys. Res. Lett.* **28**, 3501-3504 (2001).

23 Gardelle, J., Berthier, E. & Arnaud, Y. Impact of resolution and radar penetration on glacier elevation changes computed from multi-temporal DEMs. *J. Glaciol.* **58**, 419-422 (2012).

24 Nuimura, T., Fujita, K., Yamaguchi, S. & Sharma, R. Elevation changes of glaciers revealed by multitemporal digital elevation models calibrated by GPS survey in the Khumbu region, Nepal Himalaya, 1992–2008. *J. Glaciol.* **58**, 648-656 (2012).

25 Reid, T. D. & Brock, B. W. An energy-balance model for debris-covered glaciers including heat conduction through the debris layer. *J. Glaciol.* **56**, 903-916 (2010).

26 Kääb, A. Combination of SRTM3 and repeat ASTER data for deriving alpine glacier flow velocities in the Bhutan Himalaya. *Remote Sens. Environ.* **94**, 463-474 (2005).

27 Sakai, A., Takeuchi, N., Fujita, K. & Nakawo, M. Role of supraglacial ponds in the ablation process of a debris-covered glacier in the Nepal Himalayas, in *Debris-covered glaciers* Vol. 264 (eds M. Nakawo, C. F. Raymond, & A. Fountain), 119-130 (IAHS, 2000).

28 Mattson, L., Gardner, J. & Young, G. Ablation on debris covered glaciers: an example from the Rakhiot glacier, Punjab, Himalaya, in *IAHS-AISH* Vol. 218, 289-296 (IAHS, 1993).

29 Quincey, D. J. *et al.* Early recognition of glacial lake hazards in the Himalaya using remote sensing datasets. *Global Planet. Change* **56**, 137-152 (2007).

30 Immerzeel, W. W., Pellicciotti, F. & Shrestha, A. B. Glaciers as a proxy to quantify the spatial distribution of precipitation in the Hunza basin. *Mt. Res. Dev.* **32**, 30-38 (2012).

31 Rodell, M., Velicogna, I. & Famiglietti, J. S. Satellite-based estimates of groundwater depletion in India. *Nature* **460**, 999-1002 (2009).

Supplementary Information is linked to the online version of the paper at www.nature.com/nature.

Acknowledgements: We thank G. Cogley and A. Gardner for their exceptionally thorough and constructive comments. This study was supported by the European Space Agency (ESA) through the projects GlobGlacier (21088/07/I-EC) and Glaciers_cci (4000101778/10/I-AM). The study is further a contribution to the Global Land Ice Measurements from Space (GLIMS) initiative and the International Centre for Geohazards (ICG). NASA's ICESat GLAS data were obtained from NSIDC, Landsat data are courtesy of NASA and USGS, and the SRTM elevation model version is courtesy of NASA JPL and was further processed by CGIAR. A number of glacier outlines were provided by GLIMS. E.B. and Y.A. acknowledge support from the Centre National d'Etudes Spatiales (CNES) through the TOSCA and ISIS programmes, from the French National Research Agency through ANR-09-CEP-005-01/PAPRIKA, and from the PNTS. J.G. was funded through CNES/CNRS.

Author Contributions: A.K. designed the study, processed and analysed the data, created the figures, and wrote the paper. All other co-authors wrote and edited the paper and assisted in interpretations. J.G., E.B. and Y.A. provided additional data, and C.N. assisted in data processing.

Author Information Reprints and permissions information is available at www.nature.com/reprints. The authors declare no competing financial interests. Readers are welcome to comment on the online version of this article at www.nature.com/nature. Correspondence and requests for materials should be addressed to A.K. (kaeaeb@geo.uio.no).

Supplementary Information

for

Contrasting patterns of early 21st century glacier mass change in the Himalaya

Andreas Kääb, Etienne Berthier, Christopher Nuth, Julie Gardelle & Yves Arnaud

Here we provide Supplementary Methods and Discussions about

- Data preparation
- Reasons for data selection
- Computing elevation difference trends
- Division of the study region in sub-regions
- ICESat sensitivity tests and corrections
  - *ICESat waveform fitting (GLA06 vs. GLA14)*
  - *ICESat elevation sampling*
  - *ICESat saturation and slope histogram adjustment*
  - *ICESat acquisition during GLAS laser period 2F*
  - *ICESat acquisition timing*
  - *ICESat spatial sampling distribution*
- SRTM penetration, biases and voids
  - *Vertical offsets between ICESat and SRTM; radar penetration*
  - *Impact of SRTM elevation bias*
  - *Impact of SRTM void fills*
- Bedrock uplift
- Glacier definition, area estimates and associated errors
- Snow and ice densities
- Error budget for elevation difference trends and mass changes
- Comparison to other studies reporting elevation or mass changes
- Winter trends
- Thinning on clean and debris-covered ice
- Discharge estimates

with

- Supplementary Tables 1-2, Figures 1-6 with legends and References 32-78

Data preparation

All available footprint elevations from the Geoscientific LASer instrument (GLAS) during the 2003-2009 Ice, Cloud and land Elevation Satellite (ICESat) campaign[32] (~70 m footprint diameter and ~170 m along-track spacing), obtained from NSIDC (release 531; elevation products GLA06 and GLA14), are compared to the ~90-m gridded Digital Elevation Model (DEM) from the Shuttle Radar Topography Mission (SRTM) for February 2000 (void-filled version 4 from the Consultative Group on International Agricultural Research, CGIAR) through bilinear interpolation of the estimated footprint centre. About 18 % of glacier ICESat points in the study region are within the SRTM void mask and are disregarded in all further analyses unless indicated. SRTM geoid elevations are converted from the Earth Gravity Model (EGM) 1996 to EGM2008, which is used for ICESat release 531. For each footprint, elevation differences between SRTM and ICESat are computed, and SRTM slope and aspect are extracted to co-register the SRTM and ICESat data[33]. In particular, a horizontal misalignment of 0.5 SRTM pixels 45° to the northwest is found and corrected, presumably from definition problems of DEM cell origin (centre vs. corner). This misalignment is not found in the original SRTM version from JPL/USGS. Additionally, in some 1°×1° CGIAR SRTM sub-tiles, a misalignment of 2 pixels in the latitudinal direction is found and corrected. Elevation differences are re-computed after iterative alignment of the two elevation data sets. In total, ~675,000 footprint locations lie within a 10-km buffer around glaciers, including those over SRTM voids and those with potential cloud cover. (Note, that further analyses of this study are based on varying subsets of this total number, not necessarily the full sample.)

Cloud-free 30-m resolution Landsat TM or ETM scenes of the entire study region from around the year 2000 (Tab. S1) with minimal snow cover are obtained from the United States Geological Survey (USGS) in topographically corrected version (L1T) and all scenes mosaicked. The main purpose of the Landsat scene mosaic is to initially

classify ICESat footprints into ice, firn/snow, debris-covered ice, off-glacier, vegetation and water -bodies. In addition, a clean ice/firn/snow mask is derived using a ratio of Landsat Thematic Mapper (TM or ETM) bands TM3/TM5 and a threshold of 2.2 on this ratio[34] (Fig. S1) and extended by a 10-km buffer to limit the spatial analysis domain close to glaciers. The 10-km buffer also includes all debris-covered glacier sections not captured by the band ratio. Further, all available glacier outlines, mainly from the Global Land Ice Measurements from Space (GLIMS) server[35,36] at the National Snow and Ice Data Center (NSIDC), and glacier inventories over Kashmir[37] and the central Karakoram[19], are combined and compared. (Note that the ratio of debris-covered ice to clean ice/firn/snow glacier cover, which is used later for estimating the complete glacier area, is based on manually revised ICESat footprint classes, not on the glacier mask introduced here).

The digital numbers (DNs) of the individual bands of the Landsat images are extracted at each ICESat footprint location through bilinear interpolation. A Landsat band3/band5 ratio (TM3/TM5) larger than 2.2 denotes snow, firn and clean ice footprints[34]. Firn and snow are discriminated from clean ice by a threshold of ~200 on the ratio (TM4×TM2)/TM5 after stretching to values from 0 to 255. Footprints over debris-covered glacier sections are initially marked using glacier inventory outlines, where available. The footprint classifications are superimposed over the Landsat mosaic and edited manually to assign footprints to the debris-covered ice class where they are misclassified as off-glacier, to assign ice/firn/snow-class footprints outside glaciers (e.g. on small snow patches, or icings) to the off-glacier class, to correct confusion between clean ice firn/snow, and to introduce an additional water class. In total ~581,300 [526,200] footprints, of which ~477,400 [437,500] are off-glacier footprints, ~46,700 [38,200] clean ice glacier footprints, ~41,000 [35,300] glacier firn and snow footprints, ~13,000 [12,000] debris-covered glacier footprints, and ~3,200 [3,200] water footprints are obtained including [excluding] those over SRTM voids and excluding footprints

with elevation differences larger than 150 m. (Elevation differences >150 m are interpreted as indicators for cloud cover during the ICESat acquisition; more details below). Footprint classes and comparison of the clean ice/firn/snow mask with the available glacier outlines indicate consistently that ~13% of the HKKH glacier region studied is debris-covered[37-39]. Furthermore, the above footprint sample sizes suggest an accumulation area ratio (AAR) of ~40% over the HKKH for the Landsat dates used (cf. ref. 40). In addition to the clean ice/firn/snow classification, the normalized difference vegetation index (TM4-TM3)/(TM4+TM3) based on the Landsat Thematic Mapper bands 3 (TM3) and 4 (TM4) is computed for each footprint.

Reasons for data selection

Landsat data is selected from around the year 2000 rather than overlapping with the ICESat acquisitions of 2003-2009 for two main reasons. First, the failure of the Landsat7 Scan Line Corrector (SLC-off) in early 2003 resulted in data containing SLC-off voids. Second, due to the SLC failure suitable Landsat scenes after 2003 are limited requiring ~10 years to cover the entire HKKH, thus a mosaic from this data would be temporally inconsistent. The main purpose of the Landsat scene mosaic is to classify footprints into ice and firn/snow classes both for applying different density scenarios for converting elevation changes into mass changes and to estimate average SRTM penetrations. Our ICESat classification from the Landsat mosaic of ~ year 2000 provides rough regional and sub-regional AAR estimates for the HKKH (cf. ref. 40). Nonetheless, glacier areas have changed between 2000 and 2003-2009 but only by a small percentage (ref. 6, and tests within this study), very rarely affecting actual footprint classifications. Furthermore, minimal snow cover outside glaciers is of much greater importance for our study than being temporally consistent with ICESat and is much easier to observe before the SLC failure (1999-2003). Finally, we conservatively add a 10% area error to all mass budget estimates.

Two global DEMs are available to compare with the ICESat campaign: the SRTM DEM and the ASTER GDEM. Initial investigations of the GDEM (v1) revealed various high-frequency biases, such as from lack of co-registration of the stacked individual DEMs and sensor jitter[33]. The GDEM (v2) seems to be better co-registered, however, the unknown time stamp of individual elevation pixels makes this global DEM incompatible with our methods in which each ICESat laser period must be differenced to a temporally consistent DEM. The SRTM fulfils this role as the shuttle mission was restricted to 11 days in February 2000.

Computing elevation difference trends

Here, *dh* is defined as the difference between ICESat elevations (2003-2009) and SRTM elevation (2000). The *dh* trend (for 2003-2009) is defined as the trend through all *dh*.

We derive *dh* trends using a robust linear regression through all ICESat elevation differences from SRTM (i.e not a regression through the laser period *dh* medians; Figs. 2 and S2). Robust methods operate using an iterative re-weighted least squares approach in which all data points receive an equal weight for the first iteration and subsequent iterations decrease the weights on points that are farthest from the regression model until the regression coefficients converge. In our study we use the implementation by the MATLAB function `robustfit` with default parameterization. The *dh* trend represents the mean change in elevation difference over the entire ICESat acquisition period. In our approach, laser periods are implicitly weighted according to the number of footprints in them. Trends derived from laser period *dh* medians (Figs. 2 and S2), using standard regression (not shown), are mostly similar to the robust trends through all ICESat points. Largest differences, up to 0.2 m a^{-1}, occur for the JK winter trend, the KK winter trend, and the HK, HP and NB summer trends, though none of these trend differences are statistically significant, i.e. not exceeding the two combined standard errors, which are on the order of ±0.2 m a^{-1} for the standard regression using seasonal *dh*

medians, and on the order of ±0.06 m a^{-1} for the robust fit. (Remarks: error levels correspond to 1 standard error. Laser period medians are used rather than means because the median is less sensitive to outliers.)

The annual variations of laser period medians over glaciers reflect, in principle, annual glacier thickness variations. The standard errors of individual laser period means, computed as the standard deviation of *dh* for each laser period divided by the square root of the number of footprints, are, however, at least on the order of ±0.5 m, when assuming each ICESat footprint to represent an independent measurement. Any spatial autocorrelation between ICESat-derived elevations increases these standard errors significantly[41]. Therefore, we prefer not to interpret temporal thickness and annual mass balance variations within 2003-2009.

Finally, we prefer the noise-robust trend estimation based on the complete data set over using disputable *dh* filters (e.g. *n*-sigma filter) to ensure that extreme but real glacier changes (i.e. surges) are not already initially removed. However, the original histogram of *dh* exhibits two peaks, a sharp one at ~0 m and a very flat one at ~1400 m, i.e. the average cloud height above ground for the ICESat dates. The two histogram shapes intersect roughly at around 110 m. A closer examination of *dh* between the 2000 SRTM DEM and a 2008 SPOT5 HRS DEM in the Karakoram[19], a region assumed to host the largest glacier *dh* in our study area due to widespread surge activities, confirms that ±150 m is the largest expected *dh* on glaciers and thus $dh > \pm 150$ m are discarded. Also, *dh* trends computed by discarding absolute *dh* increasing from 15 m (~ 1 standard deviation of *dh*) to 150 m exhibit a low sensitivity to the exact *dh* cut-off value. The proportion of *dh* between ±15 m and ±150 m is small (11%) and the *dh* trends remain virtually stable when including differences larger than ± 20-25 m. This is mainly an effect of the small number of extreme *dh* on glaciers together with the robust regression algorithm used for trend fits, which gives a low weight to such extreme values.

Division of the study region in sub-regions

Our study region is designed to completely include all the glacier areas within the Indus and Ganges river basins. The study is then extended to incorporate glacier zones/mountain ranges in direct contact with these river basins to derive a more comprehensive regional picture of glacier thickness changes and mass budget. Consequently, glaciers in the Brahmaputra basin are only partially included; i.e. those north of Western Nepal, and in Sikkim and Bhutan. We divide HKKH into five sub-regions with approximately homogeneous glacier climates, aiming at sub-region sizes large enough to contain a sufficient spatial distribution of ICESat tracks for reasonable *dh* trend uncertainties. A further purpose of the zonation is to avoid destructive overlay of seasonal signals varying over the HKKH. The limits of the five sub-regions (Figs. 1 and S1) are mainly defined based on cell-wise *dh* trends over HKKH (Fig. 1) and on climatic information[13]. In short, we characterize glacier climate in East Nepal and West Bhutan (NB) as mainly influenced by Indian summer monsoon, and in Himachal Pradesh, Uttarakhand and West Nepal (HP) as mostly influenced by Indian summer monsoon but to a small extent also by the Westerlies. Glaciers in Jammu Kashmir (JK) are mostly influenced by the Westerlies and only to a small extent by the Indian summer monsoon. Glaciers in the Hindu-Kush section within our study region (HK) are mainly influenced by the Westerlies, but still within the extreme limits of the Indian summer monsoon. Karakoram (KK) glaciers form the northern Himalayan front, in a leeward position protected from the Indian summer monsoon, and are only influenced by the Westerlies. As these climatological and glaciological transitions are gradual, the exact boundaries between our sub-regions are subjective and cell-wise *dh* trends are therefore also given (Fig. 1).

ICESat sensitivity tests and corrections

ICESat waveform fitting (GLA06 vs. GLA14)

All analyses in this study are based on GLA14 data with up to six Gaussians fitted into the return waveform to determine footprint elevation (land parameterization). We test all elevation offsets and trends also using GLA06 data with up to two Gaussians fitted to the waveform (ice sheet parameterization)[42]. Differences are well within the error bounds, for instance with maximum *dh* trend differences of a few mm a^{-1} (maximum 0.01 m a^{-1} for KK) both for glacier and off-glacier footprints.

ICESat elevation sampling

Within each laser period, a varying elevation distribution is sampled by ICESat footprints. Since glacier thickness changes and off-glacier snow thicknesses, and perhaps also terrain-related ICESat elevation errors (see following sub-section), on average correlate to elevation, the variation of elevation sampling distributions induces a bias. This bias for individual laser periods affects the means/medians of individual laser periods, and, if systematic over the study period, also the *dh* trends. We compute a correction of such biases both for glaciers and outside glaciers from the difference between the mean elevation of an individual laser period and the mean elevation of all laser periods of the same season, multiplied by the *dh* gradient with elevation. All trends given in this study are corrected for such altitudinal biases. These biases (and corrections) become more important for smaller areas, and affect primarily the 2°×2° cells shown in Fig. 2. For our five sub-regions, altitudinal biases cause *dh* trend corrections on the order of 0.04 m a^{-1} but are statistically significant only for the winter trends of KK and JK.

ICESat saturation and slope histogram adjustment

Saturation of the ICESat return echo waveform may occur when the laser is transmitting high energy pulses to bright surfaces, which may result in pulse distortion and a delay of the pulse centre. Corrections have been derived based upon the echo return energies[43]. We conduct tests by iteratively increasing cut-offs on the ICESat saturation gain, with and without applying the saturation range correction.

i) About 50 % of all waveforms are indicated to be fully saturated (indicator value 250) (Fig. S3b). The mean off-glacier *dh* [*dh* trend] between ICESat and SRTM is -0.01 m [-0.04 m a^{-1}] for saturation indicator < 250 and +0.10 m [+0.04 m a^{-1}] for saturation indicator ≤ 250, indicating that mean *dh* and *dh* trend are different with and without fully saturated footprints included[44,45]. (Above test results include only autumn acquisitions and exclude 2F.)
ii) The percentage of saturated footprints increases notably with slope[44] (Fig. S3a).
iii) The percentage of saturated footprints is not stable over the different laser periods and exhibits even a systematic increase for laser periods 3A-K (Fig. S3b).

The combination of these three effects, that are (i) the bias in off-glacier *dh* between saturated and non-saturated footprints, (ii) the increase of the number of saturated returns with slope, and (iii) the systematic variation of the percentage of saturated returns over time, leads to a systematic variation of offsets over time and, thus, to a bias in computed *dh* trends, most pronounced for slopes > ~15°. If populations of footprints on glaciers and off-glacier had similar slope histograms, this bias could be removed by differencing glacier and off-glacier trends. In our study, however, the slope histograms for footprints on stable terrain and those on glaciers are significantly different with a histogram peak for stable terrain at ~30° slope and for glaciers at ~5° (Fig. S3c). Therefore, a slope histogram adjustment is applied for the off-glacier footprints. A maximal multiplication factor to the glacier histogram (blue dashed line in Fig. S3c) is computed so that its scaled version is still contained within the land

histogram. This multiplication factor defines the target land histogram (black dotted). For each slope bin the number of land footprints exceeding the target number (i.e. the area between the black solid and black dotted lines in Fig. S3c) is now removed by randomly eliminating footprints. As a result, the adjusted land histogram has the same shape as the glacier histogram, though vertically magnified, and contains the maximum possible number of footprints to fulfil this requirement. The procedure reduces the number of off-glacier footprints from ~526,000 to ~180,000, stabilizes the off-glacier trend at +0.00 ±0.03 m a^{-1} both for saturation indicator value < 250 and saturation indicator value ≤ 250, and reduces the difference between the *dh* means of these two footprint populations to 0.01 m. The remaining off-glacier *dh* trends for the individual sub-regions (Tab. 1) may be due to ICESat inter-campaign biases[45,46] or bedrock uplift, but are too small (< ± 0.02 m a^{-1}) and statistically insignificant to make corrections of glacier elevation trends by off-glacier trends viable. Acknowledging their unclear nature, those off-glacier trends are instead added (RSS) to the uncertainties of the glacier *dh* trends. Saturation range corrections, which are available only for a small number of footprints, have no significant effect on the glacier *dh* trends, whereas their omission even reduces the off-glacier mean *dh* slightly. From our experiments we conclude that the concepts of ICESat waveform saturation and range correction have presumably not been developed and tested for the extreme topography found in this study in particular for off-glacier terrain, and should thus not be applied for such terrain without in-depth sensitivity tests.

ICESat acquisition during GLAS laser period 2F

Laser period 2F is the last before GLAS failure. The number of footprints during 2F in HKKH is only about 10% of the average number of footprints during the other laser periods, distributed over only a few tracks. Therefore, significant differences exist in the spatial distribution (elevation, latitude, longitude) of footprints during 2F compared to the other periods. The mean elevation of 2F footprints is on average 170 m lower (up to

350 m lower for individual laser periods and sub-regions) than for the other laser periods, i.e. 2F footprints oversample glacier sections with larger glacier thickness losses than during the other periods. At the same time, comparison of 2F elevations with elevations from the other laser periods over flat terrain and lakes showed no significant elevation bias. We conclude therefore that the 2F elevations are, in principle, valid measurements, but may cause significant biases due to the reduced and biased sampling caused by the GLAS degradation. Because of this inadequate glacier sampling, we exclude laser period 2F from our analyses.

ICESat acquisition timing

In several respects, *dh* depends potentially on the timing of ICESat acquisitions. The ~June laser periods (2C, 3C, 3F) with typically highest seasonal elevations (Fig. S2) cover only the first three years of the study period (2004 to 2006), bias therefore the trend, and are removed from the trend analyses.

From the offset in mean date of the year for each laser period from the mean date of the year for all laser periods of one acquisition season (October/November= autumn and February/March = winter) over the study period, multiplied by a linear temporal trend of elevation differences for each acquisition season, we estimate that the changes in acquisition dates have a maximum effect on laser period medians or means of 0.10-0.15 m for glaciers [0.05-0.10 m for off-glacier]. This correction is too small to be visible in Figs. 2 and S2, and does not influence our *dh* trends. The dates of laser acquisitions have a maximal temporal trend (here: a delay) of +3.5 days for autumn and + 1.5 days for winter over the entire study period. The resulting maximum effect on our *dh* trends as derived from this temporal trend and the seasonal *dh* trends is +0.003 m a^{-1}, which is below the precision level of our trend estimates. Strictly, a linear temporal *dh* trend for the acquisition seasons, as used for the above sensitivity tests, is only valid roughly and only if the acquisition periods are before or after the annual elevation

minimum (for autumn) or maximum (for winter). For the winter trends this seems fulfilled as the ~June acquisitions show in most cases much higher elevations than the ~March acquisitions. For autumn, visual inspection of the Landsat and Advanced Spaceborne Thermal Emission and reflection Radiometer (ASTER) archives for snow cover distribution around the laser periods suggests that the laser acquisitions in the HKKH are typically at or after the annual elevation minimum.

ICESat spatial sampling distribution

To test the effect of incomplete spatial sampling using ICESat, we perform a bootstrapping analysis by progressively including random ICESat orbit paths (~80 orbit paths in total including ~570 individual tracks; Fig S1) and compute *dh* trends for each iteration. In total, 200 such simulations are performed for each sub-region and for the total region, and the results averaged (Fig. S4). As expected, the variability (i.e. standard deviation) of trends is in general larger than the mean standard error of trends because the latter does not contain the uncertainty from orbit representativeness with respect to the full glacier cover. The standard deviation of trends is expected to exponentially approach a stable value at some point because a steadily increasing number of hypothetical orbits, tracks and footprints will, first, eventually sample the complete study region and, second, reduce the influence of random noise. Hence, we fit (using `robustfit`) an exponential ($y=a \cdot e^{b \cdot x}$) to the variation of trends with increasing percentage of orbit paths. The intercept of this exponential with x=100% at ± 0.028 m a^{-1} [± 0.011 m a^{-1}] for glaciers [land] over the entire HKKH is then an estimate of the total error of elevation trends (Fig. S4). Since these error simulations include not only the effects of representativeness but also all other effects from spatial variations in nature and in the measurement system, together with the error of trend fit, we regard the intercept values as good indicators to test the uncertainties of our results. The errors simulated in this way for the entire HKKH and the sub-regions are similar to the statistically derived standard errors, indicating that the spatial variability of elevation

trends over the study period, and HKKH region and sub-regions, is well captured by the robust fit algorithm together with the large number of footprints, tracks and orbits available. (Note that the uncertainties given in Tab. 1 are not the statistical standard errors of trends but an error budget in which the standard errors of trends are just one component). Further, the simulation results indicate that an even lower orbit density than the actual one for the HKKH would still produce significant elevation trends, and that areas that are smaller than the complete study region or the five sub-regions can be reliably investigated, for instance the 2°×2° cells of Figure 1, though with increasing error bars.

SRTM penetration, biases and voids

Vertical offsets between ICESat and SRTM; radar penetration

ICESat elevations cannot be directly compared to the C-Band SRTM elevations mainly due to the varying penetration of the radar wave into ice, firn and snow[22,23]. Consequently, linear extrapolation of ICESat-derived glacier *dh* trends back to the SRTM acquisition date of February 2000 reveals elevation offsets of several meters (Figs. 2 and S2, Tab. S2). This linear extrapolation is however based on the assumption that temporal changes in *dh* trends between 2000-2003 and 2003-2009 are negligible. We use the average of autumn and winter *dh* trends for extrapolation assuming that the February 2000 elevation is the average of the ~October 1999 and ~March 2000 elevations, and discuss below where separate trend extrapolations for each season reveal significantly different results. The average offset over the entire HKKH is 2.1 ± 0.4 m for all glacier footprints, with significant differences among regions and land-cover classes. The offset uncertainty given is the statistical standard error of the regression constant, directly obtained by setting February 2000 as the origin of the fit ($t=0$). We cannot assess from our data the uncertainty introduced by assuming that the 2000-2003 trend equals the 2003-2009 one and any error component from this assumption would

have to be added. Bootstrapping simulations based on individual laser periods or even years (in contrast to the individual ICESat paths as used above) provide *dh* trend errors within the *dh* trend uncertainties of Table 1.

In addition to radar penetration, the offset between ICESat and SRTM could also, at least partially, be due to low-frequency biases in the SRTM vertical error[47] with respect to the ICESat elevations. As the median off-glacier offsets between SRTM and ICESat (Tab. S2) show a magnitude and spatial distribution that agrees with low-frequency SRTM biases found elsewhere[47] we find it likely that also our SRTM penetration estimates over HKKH are affected by these biases and correct all penetration estimates for it. Including such correction reduces the variation of penetration estimates over glaciers between the sub-regions significantly.

The penetration estimates using autumn and winter *dh* trends are for most sub-regions and classes statistically not significantly different. Statistically significant differences are given in Tab. S2 and reflect among others elevation changes between ~October 1999 and ~March 2000, the uncertainties in 2003-2009 *dh* trends for autumn and winter, and the exaggeration of these uncertainties when projecting them back to February 2000.

Penetrations are largest for firn/snow and smallest for debris-covered ice, and largest for KK and smallest for HP and NB. Variations of the radar penetration with sub-region and land-cover are suggested to be related to the variations in the thickness and dielectric properties of the February 2000 snow and ice penetration volume. Overall, the vertical variation of offsets agrees well with the deeper C-band penetration expected for less dense glacier facies. The February 2000 penetration is also expected to be larger on winter-accumulation type glaciers (HK, KK, JK) than on summer-accumulation ones (HP, NB).

Interestingly, the offsets over debris-covered ice and off-glacier terrain are negative in some regions, i.e. the ICESat laser appears to penetrate deeper than the SRTM C-band radar. This occurs if snow depth in February 2000 is thicker than the average for the acquisition season over 2003-2009 used for *dh* trend computation and at the same time has properties that reduce C-band radar penetration, such as meltwater in or on the snow pack. Apparent negative penetrations over glaciers may also indicate that the extrapolated 2003-2009 *dh* trends are actually not representative for the 2000-2003 glacier elevation change. For lower elevations of off-glacier terrain, experiments based on the normalized difference vegetation index suggest also that negative offsets may in parts also stem from vegetation volumes, mainly trees[44].

Given that the SRTM DEM is one of the best nearly global elevation models available so far and, hence, often used to map glacier elevation changes outside polar regions[16,19,48-51], we provide a first-order estimate to correct regionally-based elevation change measurements for average penetration of the C-band signal into ice and snow. Our regional penetration estimates compare well to other studies on C-band radar penetration[22,23,52,53].

Impact of SRTM elevation bias with elevation

The main condition that the SRTM DEM as our topographic reference has to fulfil is to contain consistent slopes. Overall elevation-dependent biases in the SRTM elevations, which are suggested to exist by some authors[50,54] and not by others[49,51,55], have little to no influence on the *dh* trends as they affect all neighbouring footprints in one orbit path in the same way. A low-frequency bias in SRTM elevation with elevation, or with latitude and longitude[47], would have the same effect as SRTM radar penetration into snow and ice and therefore does not affect *dh* trends. So, in fact our SRTM penetration estimate might be contaminated by a SRTM bias with elevation, but not our *dh* trends because SRTM elevation biases and offsets are eliminated from our trend estimation.

Any SRTM elevation bias could affect our trend estimate only if the geographic ICESat sample distribution were to change significantly and systematically over time, a possibility excluded in principle by the repeat-track nature of ICESat acquisitions, and not found for the ICESat footprints used. The existing small variations in ICESat elevation sampling are corrected for (see above section on ICESat elevation sampling).

Impact of SRTM void fills

The elevations used to fill SRTM voids show a large offset from the ICESat elevations (*dh*) of 9 m [3.5 m] for off-glacier terrain [glaciers], as expected from the fact that the elevation fills are from various sources and of unknown quality. Also the *dh* trends from SRTM void fills become unreasonable, reaching +1.8 m a^{-1} [+1.9 m a^{-1}] over off-glacier terrain [glaciers], confirming the importance of disregarding SRTM void-filling elevations in elevation change analyses.

However, exclusion of SRTM void-fill areas potentially introduces a bias in the elevations sampled, if the probability of an SRTM pixel being void varies with elevation. These sampling biases for glaciers and off-glacier terrain between raw and void-filled SRTM elevations at ICESat footprints are, however, small (Fig. S5; mean glacier elevation raw SRTM: 5295 m, mean glacier elevation with void fills: 5342 m, mean glacier elevation within void fills: 5540 m). For glaciers, this elevation sampling bias of ~50 m between the raw and void-filled SRTM corresponds to a bias in *dh* of roughly 0.2 m [0.015 m a^{-1} for *dh* trend] as derived from the average vertical gradient of *dh* [*dh* trend]. This small effect reflects among others the fact that only ~18% of the HKKH glacier area is under SRTM voids. Any elevation bias between the raw and void-filled SRTM is also part of the disagreements in the hypsometries (Figure S3d), as the ICESat hypsometries are based on the raw SRTM but the glacier mask hypsometry on the void-filled SRTM. We conclude that discarding ICESat footprints over SRTM voids does not lead to a significant bias in *dh* trends.

Over off-glacier terrain and debris-covered ice the SRTM void percentage is ~10%, over clean ice and firn/snow ~15-20%. This bias of SRTM voids away from debris-covered glacier sections has no considerable effect on our *dh* trends as trends over clean ice and debris-covered ice are found to be similar under similar geographic and topographic conditions. Our comparison of *dh* trends over clean ice and debris-covered ice is also not affected by the bias in SRTM void classes as it is based on footprint pairs.

Bedrock uplift

Our trends are not corrected for tectonic elevation changes[56,57] for the following reasons. First, the knowledge about current uplift rates in HKKH, on the order of mm a^{-1}, is limited and too unreliable for deriving a viable correction for each sub-region (ref. 12 and J.-P. Avouac, personal communication). Second, our off-glacier *dh* trends, which certainly include uplift rates, are statistically too uncertain to be used as correction. Third, the effective uplift rates underneath glaciers are uncertain. Sub-glacial erosion rates may play a significant role in parts of the HKKH and may reach the same order of magnitude as the bedrock uplift, thus partially cancelling it[26,40,58-60].

Glacier definition, area estimates and associated errors

Our Landsat clean ice/firn/snow mask uses a spectral definition of glacier areas (i.e. based on reflectance) whose main purpose is to initially classify ICESat footprints and to perform histogram comparisons (e.g. Fig. S3d). The final footprint classification, though, is obtained after manually editing this initial automatic classification. Snow patches are excluded, in particular where clearly outside of glacier terrain. Small ice areas, for instance in steep terrain, and potential ice patches that were present in the satellite images of the minimal snow cover selected were not re-classified and are thus included in our remote-sensing based glacier area estimates. Those steep ice areas and

ice patches might not be included in conventional map-based glacier inventories. In that respect, our study investigates rather the mass balance of the perennial surface ice reserves in the HKKH (and snow reserves where we assumed that ice underlies the snow). Due to the steep topography in the study region, areas above the glaciers are known to contribute significant mass to the glaciers through ice and snow avalanching[8,40]. We therefore consider areas that are snow or ice-covered under minimal snow conditions of our Landsat mosaic to be part of the glacier mass balance system of the study region, and included them in our glacier area estimate.

In order to test the influence of our above definition of glacierized area on the *dh* trends we remove for subsets within the five sub-regions all glacier ICESat footprints that might not be included in traditional map-based glacier inventories. In detail, we keep only footprints that can clearly be assigned to a glacier and remove in particular footprints (i) on steep flanks where the connection to the main glacier is unclear, (ii) ice patches and snow remnants that were initially interpreted as being perennial, and (iii) debris-covered glacier parts that may actually be ice-cored moraines or transformed into rock glaciers. In all sub-regions, this footprint restriction leads consistently to removal of ~25% of our initial glacier footprints. For HK, KK and JK the footprint removal has no significant effect on the *dh* trends. For HP the trend after removal increases by 25% (from -0.38 m a^{-1} to -0.48 m a^{-1}), for NB by 50% (from -0.38 m a^{-1} to -0.56 m a^{-1}). The distribution of effects from glacier footprint restriction on *dh* trends with no change in the west and increasing changes towards the east is not surprising. The Landsat scenes used for classification stem from the late summer for the western sections that contain winter-accumulation type glaciers (Tab. S1), i.e. the season with clearly minimal snow cover. For summer-accumulation type glaciers in the east, the season of minimal snow cover is not well defined, and frequent fresh snow and cloud cover during the monsoon season forces the use of winter Landsat scenes (Tab. S1) that potentially contain more snow cover outside glaciers.

For the entire HKKH the *dh* trend over a more conservatively defined glacier area might thus be ~10% more negative [-0.29 m a^{-1} instead of -0.26 m a^{-1}]. This difference is on average statistically not significant and thus confirms the robustness of our *dh* trend and its error bounds, but should be kept in mind when comparing our results for HP and NB to other regional measurements of glacier volume or mass changes. Further, the ~25% footprints found not to belong to glaciers in a strict and clearly identifiable sense but rather to belong to the HKKH surface ice cover, suggests that the glacier area in a strict sense might be ~20% smaller than our estimate of ~60,000 km^2. This area reduction would also reduce our glacier mass change estimates (mass budget, SLE, discharge equivalent) accordingly. However, the sections excluded in the more restrictive glacier area definition contribute also to mass changes[12] and run-off, and we prefer therefore to base our final results on our more expansive definition of glacierised area[61].

Our final area estimate is obtained by scaling the ratios between total sub-region areas and total number of footprints in them, i.e. the inverse footprint density, with the number of footprints in the glacier class. The areas for debris-covered ice and snow/firn are computed analogously (Tab. 1). The glacier areas obtained by that approach are ~2.5% smaller than the areas from the Landsat clean ice/firn/snow mask (including a correction for average debris-cover percentage). This discrepancy is mainly due to the manual removal of ICESat footprint classifications over obviously temporary snow fields that remain in the spectrally defined glacier mask.

Errors in glacier area, if due to misclassifications of glacier as land, or vice-versa, can also influence the *dh* trends. If distributed over the entire study region, a systematic average land-to-glacier or glacier-to-land misclassification error of, for instance, 5% will change the glacier *dh* trend over the entire HKKH by only 5% of this trend, that is 0.01 m a^{-1}. The effect of random misclassifications in both directions, which are more

likely, will be even smaller than the effect of systematic misclassifications. Misclassifications between ice and firn/snow affect the proportion of footprints assigned to a given density and are discussed below in the section on ice and firn/snow densities.

Within the polygon defining our study region (Fig. S1), the extended World Glacier Inventory[62] (WGI-XF) contains a glacier area of 51,200 km^2 , versus 60,100 km^2 from our estimate based on up-scaling of ICESat footprint classifications. The WGI-XF estimates are based on maps from the 1970s to ~2000, and therefore, due to area loss, the WGI-XF areas should be even larger than our estimates from ~2000. We attribute the significant discrepancy between both area estimates to the following reasons. First, our estimate is, as a reflectance-based one, expected to be larger than a conventional map-based one, by up to ~20% (see above). Second, the WGI-XF over our study region contains a number of larger and smaller voids. Third, an independent remote-sensing based glacier inventory over Kashmir[37] alone contains 20,770 [WGI-XF over the same region: 9] glacierets and ice patches with an area ≤ 0.01 km², 18,800 [154] between 0.01 and 0.05 km², and 12,450 [572] between 0.05 and 0.1 km². Based on that, we estimate for the entire HKKH that the underrepresentation of glacierets and ice patches[61] in the WGI-XF alone could explain an area difference of roughly 2000-3000 km^2 between our estimate and the WGI-XF. Based on the above reasons, we prefer to not use the WGI-XF as area estimate (see also ref.61).

A recently published glacier outline compilation[36] over our study region (Randolph Glacier Inventory, RGI) contains a glacier area of 49,500 km^2 for our study region, though with a considerable number of smaller and larger gaps that become obvious when superimposing the outlines on our Landsat mosaic.

A thorough glacier inventory over Kashmir[37] (parts of JK and HP) based on ~ year 2000 Landsat data, and satellite L-band radar coherence for detecting debris-covered ice, contains 9450 km^2 of glaciers, while our area estimate is 9150 km^2, a

difference of only 3%. In acknowledgment of the differences between our area estimate, the RGI and the WGI-XF, we introduce a ±10% glacier area uncertainty in the mass budget, discharge equivalent and SLE estimates.

Snow and ice densities

The total mass change calculations (total mass budget, discharge equivalent, SLE) are affected by the assumptions for snow and ice densities. About 75% of the 2003-2008 autumn volume change occurred below the mean glacier elevation [85% below the ~year 2000 firn and snow line], so that uncertainties in assuming firn/snow or ice density for the accumulation areas have a limited impact on our estimates. We apply two different density scenarios (Tab. 1). Scenario (a) assumes a density of 900 kg m^{-3} for all elevation differences, certainly reasonable for areas below the firn and snow line, and thus satisfied for ~75-85% of the volume change. Scenario (a) is equivalent to assuming no changes in the vertical density profiles down from surface[63], and that volume changes in the accumulation areas happen through ice dynamics. Scenario (b) assumes a density of 900 kg m^{-3} for areas classified as ice in the Landsat images around year 2000, and a density of 600 kg m^{-3} for areas classified as firn and snow[64,65], equivalent to an AAR of 40% (Tab. 1). This scenario assumes all elevation changes over firn and snow result from changes in the density profile, with no dynamical component involved in the elevation differences. This scenario might, for instance, apply if glaciers during our observational period are exposed to exceptional melt conditions (sub-region JK?), so that formerly perennial firn and snow volumes are lost[66], or for thickness increases due to increased accumulation (sub-region KK?).We believe therefore that the most realistic mass budget estimate is the mean of scenarios (a) and (b), and we add (RSS) the standard deviation of the mean of the two scenarios to the total error in mass budget.

In addition to uncertainties related to the application of ice or firn/snow densities to accumulation areas, our density estimates (and partially also *dh* estimates) are potentially affected (i) by the uncertainty whether the ~ year 2000 firn/snow areas are representative for the ICESat period, (ii) by uncertainties of the densities used (900 kg m^{-3} for ice and 600 kg m^{-3} for firn/snow), and (iii) by the possibility that ICESat autumn acquisitions do not capture the minimum seasonal elevation; additional snowfall or melt may have occurred before or after the laser acquisitions. We visually examine the Landsat and ASTER data archives for the ICESat autumn periods and find mainly only minor or no fresh snow cover on the glaciers, without a clear temporal trend that would affect our *dh* trend. Further, we simulate the effect of new snowfall before or additional melt after the autumn acquisitions by adding to the heights of each individual laser period a random Gaussian distributed thickness with zero mean and ±0.1 m standard deviation. As calculated from the average *dh* trend or the elevation gradient of *dh* trend, respectively, this thickness uncertainty corresponds also to a density uncertainty of about ±10-30% (average 20%) of the density values used, a firn/snow line elevation uncertainty of about ± 300 m, or an AAR uncertainty of ±20% (i.e. AARs ranging from 20-60%). From 100 iterations of trend estimations, we find a variation of *dh* trends of ±0.02 m a^{-1}, and add this uncertainty to our overall error budget of *dh* trends and derived mass changes.

Error budget for elevation difference trends and mass changes

Error levels correspond to 1 standard error. The total error budget for the *dh* trends is computed as the root of sum of squares (RSS) of

- standard errors of the parameters as fitted using the robust regression algorithm. The standard errors of trends cover erroneous *dh* from random vertical SRTM or ICESat errors, and the natural variability of glacier thickness changes at footprint locations;

- off-glacier *dh* trends as their nature is unclear and they might reflect spatial biases in *dh* trends;
- the simulated *dh* trend uncertainty due to melt after and snowfall before ICESat autumn acquisition.

In addition, the derived mass changes (Gt a^{-1}, WE, SLE, discharge equivalent) contain (RSS):

- the effect of a 10% glacier area uncertainty;
- the standard deviation of the mean of density scenarios (a) and (b).

Uncertainties in density values used and in firn/snow line position are already covered by the simulated effect of *dh* offsets for autumn laser periods.

Comparison to other studies reporting elevation or mass changes

We compare our 2003-2008 autumn *dh* trends with other estimates available for different parts of the HKKH. We obtain -0.77 ± 0.08 m a^{-1} for a 2° latitude × 2° longitude cell around a smaller region in the Himachal Pradesh where -0.78 to -0.95 m a^{-1} elevation change (range of possible *dh* given) was found between 2000 (SRTM) and 2004 (satellite stereo)[16]. In the same region, the directly measured mass balance of the 16.5 km² Chhota Shigri Glacier, the largest glacier with consistent ongoing direct mass balance measurements in the HKKH and situated in the middle of the above cell, averages to -0.88 ± 0.4 m a^{-1} WE over 2003-2008 (ref. 20; Fig. S6; accuracy at 1 standard error level[67]).

For a 2°×2° cell around Mt. Everest (~ 2,700 km^2 of glaciers) we find -0.41 ± 0.14 m a^{-1} elevation change over 2003-2008 against -0.87 ± 0.58 m a^{-1} (-0.79 ± 0.52 m a^{-1} WE specific mass balance) over 2002 to 2007 at a smaller study region (~50 km^2 glacier) from satellite stereo[17]. (Note that a more conservative definition of glacier areas compared to our mostly spectrally-based definition leads to ~50 % larger elevation

losses in the NB sub-region; see above section on glacier areas). Our value (-0.41 ± 0.14 m a^{-1}) is in better agreement with the DEM-derived mean elevation changes (-0.47 ± 0.29 m a^{-1}) for 183 km^2 of glaciers in the Khumbu area during 1992-2008 (ref. 24), over a longer time period though.

In the central Karakoram, the sub-region within HKKH believed to host the largest variability in elevation changes due to widespread glacier surging[68], we obtain for a 1°×1° sized cell -0.09 ± 0.09 m a^{-1} [-0.06 ± 0.08 m a^{-1} for a 2°×2° cell around the region] from 2003-2008 ICESat versus +0.12± 0.25 m a^{-1} between 2000 (SRTM) and 2008 (satellite stereo; similar size to that of our 1°×1° cell; 5,600 km^2 glacier area)[19]. We note that our ICESat-derived trends in this region are particularly sensitive to the location of the cell centre and the cell size, indicating a large spatial variability of *dh* trends, among others presumably due to widespread variations in glacier dynamics[68,69]. For this region, we also tested the representativeness of ICESat footprints by sampling the DEM-derived map of *dh* solely along ICESat tracks. The along-ICESat only (+0.19 ± 0.62 m a^{-1}) and full-DEM (+0.12 ± 0.25 m a^{-1}) regional *dh* trends differ by only 0.07 m a^{-1}, which is within the statistical error of our ICESat-trends and indicates thus representative ICESat tracks even in this region of surge-type glaciers.

The geodetic mass balance over ~ 1998-2009 for three small glaciers in Nepal[18] (AX010, 0.4 km^2, and Yala, 1.9 km^2, within our sub-regions NB, and Rikha Samba, 4.6 km^2, within HP but close to NB) was found to be -0.81 and -0.80 m WE a^{-1} for the two smaller ones and -0.48 m a^{-1} WE for the larger one with uncertainties of ~±0.08 m a^{-1} WE for AX010 and Yala, and ~±0.05 m a^{-1} WE for Rikha Samba. The mass balance of the largest glacier of the three, Rihka Samba, statistically agrees with our results when the correction factor for a more strict definition of glacier areas is applied (25% for HP and 50% for NB). It is to be expected that the mass balances of the two smaller glaciers

are significantly more negative than our regional average[10,70]. (For an overview of other mass balance measurements in the Himalayas see ref. 5).

Our ICESat-derived *dh* trends and the above studies agree all within their statistical significance levels, except for the very small Yala and AX010 glaciers. Though, it should be noted that, first, the study periods compared are different, which may introduce a substantial error (see annual variations in Figs. 2 and S2, and ref. 12). Second, most of the above comparison studies are based on photogrammetry that typically has problems with steep glacier sections such as glacier margins and ice falls that are therefore often not completely represented in the *dh* maps or erroneous causing *dh* biases[71,72]. Third, the photogrammetric problems over low-contrast sections (snow) typically result in an under-sampling of accumulation areas, and in larger elevation uncertainties in these zones.

Our 2003-2008 HKKH mass budget of -12.8 ± 3.5 Gt a^{-1} (1 standard error level) is much more negative than a recent estimate of -5 ± 3 Gt a^{-1} based on satellite gravimetry[12] (GRACE) over 2003-2010 (1 standard error level; note that ref. 12 originally give their uncertainties at 2 standard error levels, i.e. -5 ± 6 Gt a^{-1}). The two studies do not spatially and temporally overlay perfectly. The Himalaya region of the GRACE study (Himalaya and Karakoram) extends more to the east, a region where we find pronounced mass losses, and less to the west, a region where we and the GRACE study (its Pamirs and Kunlun Shan zone) find small mass changes. Both effects increase the difference between our ICESat-based and the GRACE-based estimates. Also, the observation periods of both studies do not perfectly coincide. For Jan 2003 – Dec 2007 the GRACE-based study suggests a glacier mass change in the Himalaya and Karakoram of -3 ± 6 Gt a^{-1}, for Jan 2004 – Dec 2008 one of -2 ± 5 Gt a^{-1}, and for Jan 2005 – Dec 2009 one of -14 ± 5.5 Gt a^{-1} (all uncertainties from ref. 12, which are originally given at 95% confidence interval, converted to 1 standard error level). The

large temporal variability in gravity changes is also noted[12] but does not help to reconcile both estimates. Our data do not show a massive decline in glacier elevation in the second part of the study period, although ICESat data only extend until the beginning of 2009. An unrealistic density of ~300 kg m^{-3} for the ICESat-derived thickness changes, equivalent to settled fresh snow, would be required to bring our mass change estimates into agreement with the GRACE-derived one. This density scenario is too unrealistic given that 75-85% of the observed volume loss occurs in the glacier ablation areas, and given that our off-glacier winter trends show no pronounced trends in snow thicknesses. It is beyond the scope of our study to discuss satellite gravimetry and potential error sources of the GRACE-based glacier mass change estimates. Such error sources are discussed in detail within ref.12. Rather, we see a large potential of satellite gravimetry to better detect large-scale sub-surface mass changes such as from hydrology or tectonics by relying on glacier mass changes from studies such as ours. In that context it should also be noted that our study provides (through surface elevation changes) mass changes of surface ice occurrences, but is not able to resolve changes in ground ice mass in permafrost zones[73].

Winter trends

Elevation change trends through the ICESat laser campaigns in autumn (~October-November) represent annual glacier mass balances. The difference between autumn and winter trends (~March) is related to changes in mass turnover (Fig. S2). (Note that winter thickness changes have a 2-3 times lower density than autumn ones.) The comparison between autumn and winter trends is further complicated by the fact the ICESat winter trends (~March) do not sample the maximum seasonal snow thickness, as indicated by the higher elevations during the ~June acquisitions (Fig. S2). The winter trend in NB is virtually identical with the annual trend expressing the summer-accumulation glacier type in this sub-region that lacks separate accumulation and

ablation seasons. In JK, the winter trend is, even without correcting for the density differences, less negative than the autumn trend indicating an increasing mass turnover, i.e. a combination of increasing ablation and accumulation. Increasing accumulation by increasing winter snow depth is also suggested by a winter off-glacier trend of $+0.21\pm0.05$ m a^{-1} in JK, the only sub-region with a winter off-glacier trend that is significantly different from zero. This positive winter off-glacier trend may indicate increasing snow depths, and thus increasing glacier accumulation and mass turnover, when assuming that the trend is not due to a change in snow fall timing. The difference between autumn and winter trends in HP marks a transition between the regimes found in NB and JK, and the elevation offset between both trends is a sign of seasonality. Considering density differences of factor 2-3, the winter trend in HK is roughly parallel to the autumn trend suggesting no significant changes in mass turnover in this sub-region. In KK, the positive winter trend and the slight negative autumn trend imply a slightly increasing mass turnover, though we acknowledge a complex impact of changes in precipitation[74], temperature[9] and ice dynamics on the KK glaciers[8,19,75]. The effect seems to be concentrated in the extensively glacierised upper elevation zones[8,14], as the winter off-glacier trend, which in the KK mainly samples low altitudes, or steep avalanche-prone terrain[8] where snow pack thickness is limited, is indiscernible from zero. An increased mass turnover in KK is consistent with the observation of gradual acceleration of a number of large KK glaciers[69,76].

Thinning on clean and debris-covered ice

The comparison between *dh* over clean and debris-covered ice is complicated by a number of biases between both samples. Footprints over debris typically have much lower mean elevations than clean ice ones, causing a vertical *dh* bias between both footprint classes. The geographic distributions of debris footprints and clean-ice footprints are not identical, so that they might reflect different local climates. Similarly,

the two samples represent different slopes and aspects, both playing a dominant role for incoming short-wave radiation and thus impacting on ice ablation. All these biases are connected through topography. We find the elevation bias, as expected, and the aspect bias to be the largest ones in our study region. The strong aspect bias suggests that, on average, the debris-cover percentage is significantly higher on southfacing glaciers than on northfacing ones, and is similar for west- or eastfacing ones[26,40].

In response to the above biases and their topographic interdependencies we construct footprint pairs of clean and debris-covered ice. For each debris-covered ice footprint all clean-ice footprints with an altitude difference < 50 m, a geographic distance < 2 km, a slope difference < 5°, and an aspect difference < 45° are selected, and the one with the smallest geographic distance chosen as matching partner for the pair. The average distances in topographic feature space are, though, much smaller than the chosen thresholds, for instance 1.1 km for the horizontal distance or 10 m for the altitude difference. Quantitatively, the final results depend on the exact thresholds defined, but are qualitatively robust against moderate variations in these thresholds. Obviously, results are most sensitive to a substantial increase in the altitude threshold, which is therefore kept at a reasonable minimum (50 m; effective average altitude difference: 10 m). The more restrictive the thresholds, the fewer pairs fulfil the defined topographic similarity and the more uncertain the results become. Each point is assigned to at most one point of the other class, and only points from autumn laser periods are used. Finally, robust trends for the pairs are computed for each of the two land cover classes (clean and debris-covered ice) and each of the five sub-regions (Tab. 1).

Comparing elevation differences over debris-covered ice to ones over clean ice cannot strictly reveal if differences stem from melt rates being different over both classes or from spatial variations in glacier dynamics (i.e. variations in divergence of flux). However, the mean distance between footprint pairs of ~1 km, and the visual

confirmation that pairs are typically located on the same glacier, suggests that the differences should at least to some extent reflect differences in ablation rates, rather than substantial ice-dynamical variations within a footprint pair.

Whereas debris thicknesses larger than ~ 0.03 m are known to insulate and thus reduce ice melt beneath them, debris or dust covers thinner than ~ 0.01 – 0.03 m increase ice melt due to effects from albedo increase exceeding the insulation effects[25,77,78]. Thus, reduced lowering due to reduced ice melt under debris is not necessarily expected under all conditions, and our finding of, on average, similar *dh* trends for clean and debris-covered ice is in principle a mixed signal composed of reduced melt under thick debris covers and increased melt under thin debris and dust covers. Both, footprints classified as clean or debris-covered ice can contain thin debris and dust layers, depending on the cover fraction, debris/dust density, its spectral properties and our band ratio threshold, so that elevation changes on both classes are potentially affected in a similar way. Further, we regard a patchy distribution of thin and thick debris/dust covers as an expression of thermokarst, which we in general assume to be the main process family behind the comparatively high lowering rates on debris-covered ice. It remains to be investigated to what fraction effects from debris thickness variations may be responsible for our findings compared to other thermokarst processes such as melt ponds[27]. To our best knowledge, no suitable study of debris thickness variations over the scale of entire glacier tongues is available in the HKKH to better constrain our interpretation.

Discharge estimates

We compare our discharge equivalent glacier imbalance 2003-2008 to published discharge estimates for the study region. Ref. 13 model discharge (discharge = rainfall + snowmelt - evapotranspiration) for the outlets of Himalayan catchments, i.e. catchments

with high mountains and, typically, glaciers in them. These combined Himalayan catchments are indicated in Figure S1. We compare our discharge equivalent glacier imbalance to the discharge sum over the Himalayan catchments Upper Indus, Jhelum, Chenab, Ravi, Beas, Sutlej (Indus basin), and Tons, Ganges, Mahakali, Karnali, KaliGandaki, Seti, Marsyandi, Trisuli, Sunkosi, Arun, Tamur (Ganges basin)[13]. For the combined Himalayan catchments of the Ganges[13] with a glacier area of ~16,500 km^2 (9% of the total area of 181,872 km^2 for the combined mountain catchments), we obtain a glacier mass balance of -0.35 ± 0.08 m a^{-1} WE (185 ± 45 m^3 s^{-1}), and ref. 13 provides a total annual average discharge of 8,200 m^3 s^{-1}. Our calculations for the combined Himalayan catchments of the Indus basin with a glacier area of 31,000 km^2 (10% of the total area of 319,980 km^2 for the combined mountain catchments) results in a glacier mass budget of -0.30 ± 0.04 m a^{-1} WE (300 ± 53 m^3 s^{-1}). For the same system of catchments, ref. 13 obtains a total annual average discharge of 8,200 m^3 s^{-1}. (Note: the discharge estimates for the mountain catchments of the Indus and Ganges basins are equal by coincidence). The glacier mass balance within the Indus basin (-0.30 ± 0.04 m a^{-1} WE) seems surprisingly negative given the fact that this basin includes parts of Karakoram with its stable mass budget. This is because thickness gains in KK occur according to our study (cf. ref. 19) actually north of the Indus basin (autumn: +0.14 ± 0.06 m a^{-1}; winter: +0.52 ± 0.07 m a^{-1}) and do not contribute to the Indus basin glacier mass imbalance.

For our discharge comparisons of the Upper Indus basin (Fig. S1) containing a glacier area of 25,000 km^2 (12% of the total basin area of ~200,000 km^2), we obtain a glacier mass balance of -0.29 ± 0.05 m a^{-1} WE and discharge equivalent of ~231 ± 46 m^3 s^{-1}. This value compares to a total annual average river discharge of 4,200 m^3 s^{-1} (ref. 13) or 2280 m^3 s^{-1} (ref. 14). The latter discharge value is similar to the average discharges measured at Terbala dam and Besham Qila (Fig. S1). It is beyond the scope of this study to discuss which of the two discharge estimates that are based on different

input data, different hydrological models, different time periods, different river discharge observations for validation/tuning, and slightly different basin outlines, might be better suited for comparison to our glacier imbalance discharge equivalent.

Supplementary Tables and Figures

Supplementary Table S1: List of the maximal snow-free Landsat scenes used in this study. Note the shift of dates from east to west due to different climatic seasonality.

Landsat no.	Landsat path/row	Scene date	Sub-region
7	137/41	28.12.2000	NB
7	138/40	19.12.2000	NB
7	138/41	19.12.2000	NB
7	139/41	08.11.2000	NB
7	140/40	05.01.2002	NB
7	140/41	05.01.2002	NB
7	141/40	22.11.2000	NB
7	142/40	15.12.2000	HP
7	143/39	03.10.2000	HP
7	143/40	09.12.2001	HP
7	144/39	13.10.2001	HP
7	145/38	02.11.2000	HP
7	145/39	01.08.2001	HP
5	146/36	24.08.1998	KK
7	146/37	21.08.2000	KK
7	146/38	09.09.2001	HP
7	146/39	05.08.2000	HP
7	147/35	02.08.2002	KK
7	147/36	02.08.2002	KK
7	147/37	02.08.2002	JK
7	147/38	02.08.2002	HP
7	148/35	21.07.2001	KK
7	148/36	04.09.2000	KK/JK
7	148/37	17.08.1999	JK
5	149/34	13.08.1998	KK
5	149/35	13.08.1998	KK/HK
5	149/36	29.08.1998	JK/HK
7	150/34	02.09.2000	HK
7	150/35	16.09.1999	HK
7	151/34	30.08.2002	HK
7	151/35	30.08.2002	HK

Supplementary Table S2: Penetration of SRTM C-band radar waves as estimated from extrapolating the ICESat elevation difference trends to the SRTM acquisition time in February 2000. Mean of autumn and winter/spring trends used for linear extrapolation. Seasonal trends that lead to significantly different penetration estimates are given in parentheses. Positive numbers indicate SRTM penetrates deeper than ICESat projected to February 2000. All penetration estimates are corrected for the median vertical off-glacier offset (numbers in parentheses below the off-glacier penetration estimate). Error level given is 1 standard error.

SRTM penetration (m)	*Hindu-Kush (HK)*	*Karakoram (KK)*	*Jammu Kashmir (JK)*	*Himachal Pradesh, Uttarakhand and West Nepal (HP)*	*East Nepal and Bhutan (NB)*	*Area-weighted mean (HKKH)*
Off-glacier (median)	0.1 ± 0.4 (-0.2)	-0.2 ± 0.2 (0.9)	0.6 ± 0.2 (0.6)	0.1 ± 0.2 (-0.5)	-0.2 ± 0.2 (-2.0)	0.0 ± 0.2 (-0.1)
Glacier (autumn / winter)	2.4 ± 0.4 (1.0 / 4.0)	2.4 ± 0.3 (3.6 / 1.3)	1.4 ± 0.6	1.5 ± 0.4 (1.0 / 2.0)	2.5 ± 0.5	2.1 ± 0.4
Firn/snow (autumn / winter)	5.1 ± 0.7 (2.2 / 8.0)	5.5 ± 0.3 (6.1 / 4.9)	2.3 ± 0.9	2.3 ± 0.6 (3.4 / 1.2)	4.8 ± 0.7	4.3 ± 0.5
Clean ice (autumn / winter)	1.7 ± 0.6 (0.4/ 3.0)	1.1 ± 0.5 (2.0 / 0.2)	1.7 ± 0.7	1.7 ± 0.6 (-0.1 / 3.4)	0.1 ± 1.2	1.2 ± 0.6
Debris-covered ice	2.0 ± 0.8	-2.9 ± 0.9	2.0 ± 1.1	0.4 ± 0.8	-0.8 ± 1.0	-0.6 ± 0.9

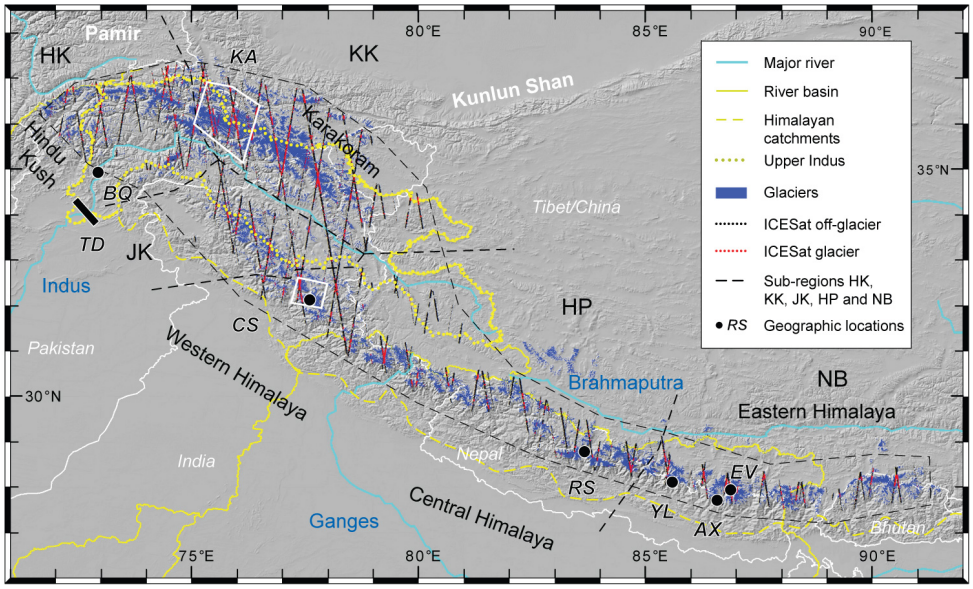

Supplementary Figure S1: Glacier mask over the Himalayas compiled from a band ratio based on Landsat satellite imagery and existing glacier inventories/outlines. All ICESat footprints are indicated. The yellow dashed line indicates combined Himalayan catchments[13], the yellow dotted line the Upper Indus basin[13,14]. TD: Tarbela dam, BQ: Besham Qila, KA: white polygon of Karakoram study region of ref. 19, CS: Chhota Shigri Glacier and white polygon of study region of ref. 16, RS: Rikha Samba, YL: Yala, AX: AX010, EV: Mt. Everest,

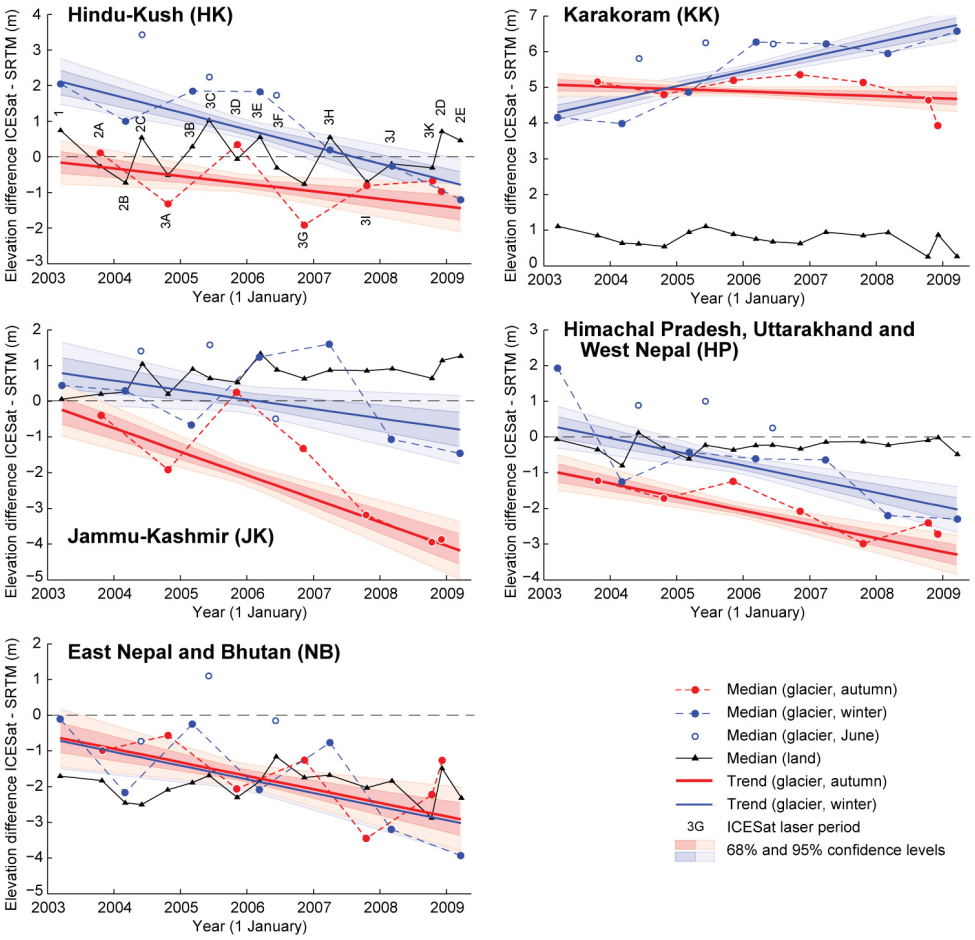

Figure S2: Median elevation differences between ICESat and SRTM for each ICESat laser period and glacier elevation difference trends for the five sub-regions defined in Figure S1. Black triangles (land), filled blue dots (winter), blue dots with white fill (~June) and red dots (autumn) are median elevation differences for each laser period (1, 2A-E, 3A-K). Autumn trends (red lines) and winter trends (blue lines) are fitted through all individual elevation differences using a robust fit method. Vertical offsets from zero obtained by extrapolating ICESat-trends to the SRTM acquisition date of February 2000 are mainly an expression of SRTM C-band radar penetration into snow and ice.

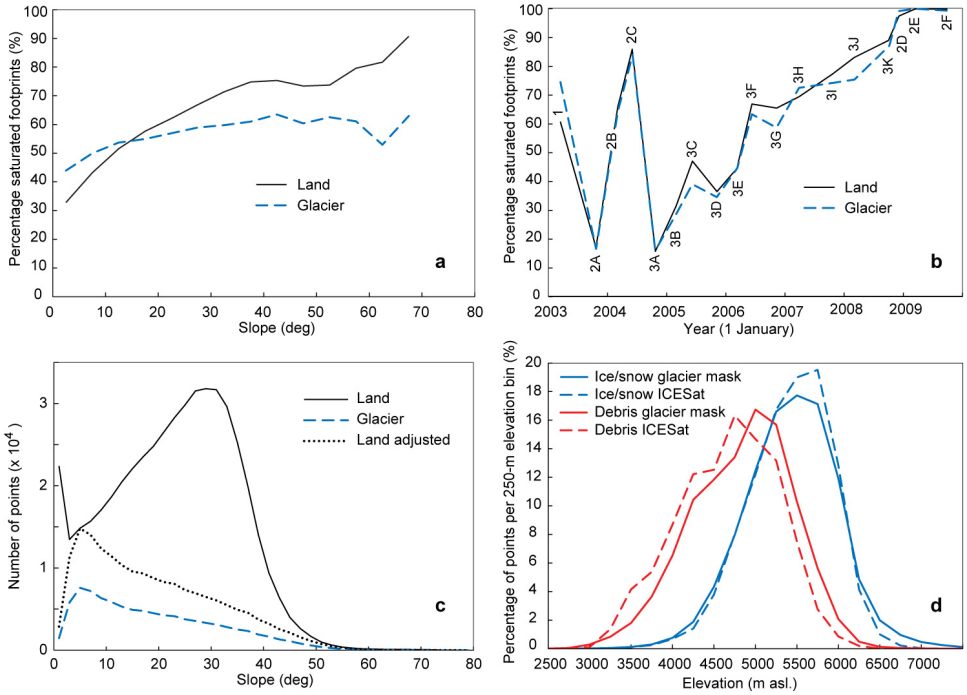

Supplementary Figure S3: ICESat footprint distributions. a) The percentage of fully saturated waveforms increases with slope, in particular for off-glacier terrain (land). b) The percentage of fully saturated ICESat waveforms also varies with time and increases systematically from laser period 3A on. Effects a) and b) together with an elevation bias between saturated and unsaturated footprints leads to a bias in elevation differences over time, i.e. a spurious trend, which is removed by adjusting the off-glacier (land) footprint histogram with slope to the glacier histogram (panel c). d) While the elevation histograms of ICESat footprints of glacier snow and ice overlap well with the altitude histogram for all snow and ice areas from the glacier mask, there is a small offset between the two corresponding histograms for debris-covered ice. We attribute that to the fact that our glacier mask is not complete for debris-covered ice in particular at low elevation. In total, however, both histogram sets overlap well enough to extrapolate ICESat-derived elevation differences to the total glacier cover. Note that the debris-covered areas correspond only to 13% of the total glacier area in HKKH.

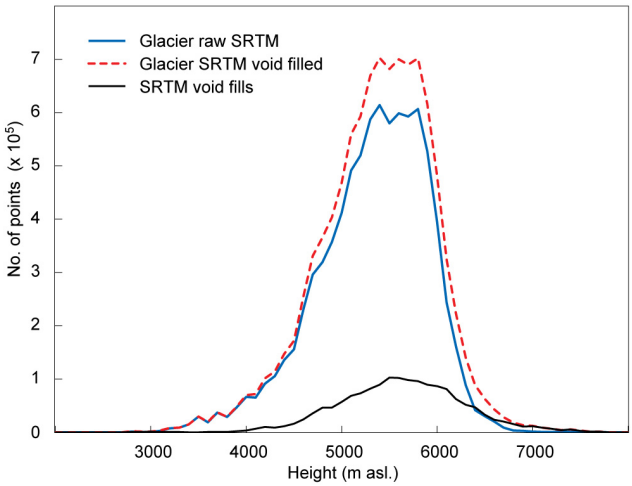

Supplementary Figure S4: SRTM elevation histograms at ICESat footprints over glaciers with and without SRTM voids.

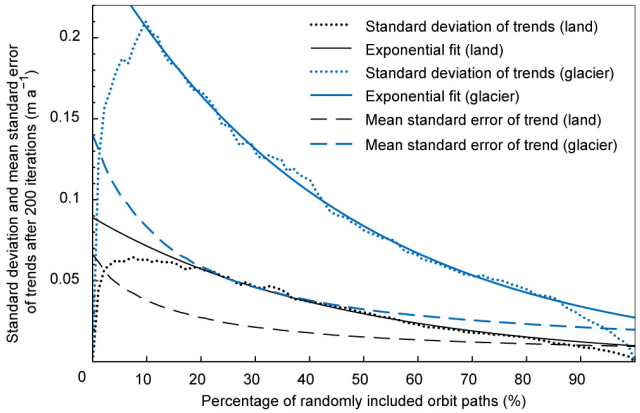

Supplementary Figure S5: Simulation (bootstrapping) of accuracy of elevation difference trends. Random orbit paths are cumulatively included in the trend computation up to the full set available for the study region. The mean standard error of trends, here shown after 200 such simulations, is lower than the variability of trends (standard deviation), because the latter includes not only the goodness of fit but also the representativeness of ICESat orbit paths. The standard deviation of trends with increasing number of orbit paths resembles an exponential, the intercept of which at x=100% is considered to be a validation for the mean standard error of trend used in this study as one component of the error budget of *dh* trends. The similarity of standard error and standard deviation intercepts indicates that the combined number and distribution of ICESat footprints is representative over the study region.

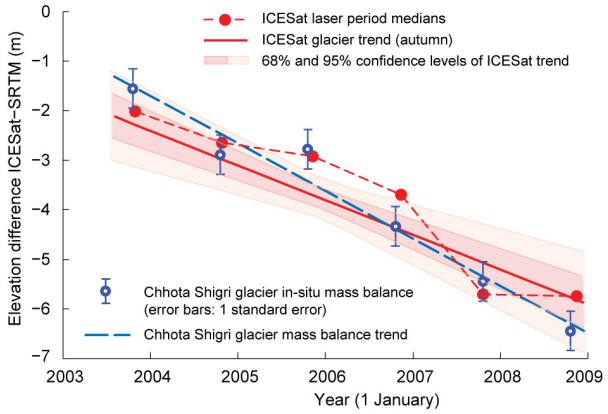

Supplementary Figure S6: Chhota Shigri Glacier in-situ cumulative mass balance[20] and ICESat-derived trends of a 2° x 2° degree cell around it. The Chhota Shigri Glacier mass balance is converted to elevation change using a density of 900 kg m^{-3}. Laser periods 3K and 2D (both autumn 2008 but a few weeks apart) have been averaged to one. The Chhota Shigri series starts in autumn 2003 with the 2002-2003 mass balance (converted to elevation change). The error bars given for the Chhota Shigri mass balance measurements correspond to 1 average standard error of an annual mass balance as estimated by ref. 20 and 67. Note that the ICESat *dh* trend line (red line) is not the regression through the shown laser period medians (red dots) but rather derived from all ICESat footprints using a robust fit.

Supplementary References

32 Zwally, H. J. *et al.* ICESat's laser measurements of polar ice, atmosphere, ocean, and land. *J. Geodyn* **34**, 405-445 (2002).

33 Nuth, C. & Kääb, A. Co-registration and bias corrections of satellite elevation data sets for quantifying glacier thickness change. *Cryosphere* **5**, 271-290 (2011).

34 Paul, F., Kääb, A., Maisch, M., Kellenberger, T. & Haeberli, W. The new remote-sensing-derived Swiss glacier inventory: I. Methods. *Ann. Glaciol.* **34**, 355-361 (2002).

35 Raup, B. *et al.* Remote sensing and GIS technology in the global land ice measurements from space (GLIMS) project. *Comput. Geosci.* **33**, 104-125 (2007).

36 Arendt, A. *et al. Randolph Glacier Inventory [v1.0]: A dataset of global glacier outlines*. (Global Land Ice Measurements from Space, Boulder Colorado, USA. Digital Media, 2012).

37 Frey, H., Paul, F. & Strozzi, T. Compilation of a glacier inventory for the western Himalayas from satellite data: methods, challenges and results. *Remote Sens. Environ.* , in press (2012).

38 Nuimura, T. *et al.* Temporal changes in elevation of the debris-covered ablation area of khumbu glacier in the Nepal Himalaya since 1978. *Arct. Antarct. Alp. Res.* **43**, 246-255 (2011).

39 Bhambri, R., Bolch, T., Chaujar, R. K. & Kulshreshtha, S. C. Glacier changes in the Garhwal Himalaya, India, from 1968 to 2006 based on remote sensing. *J Glaciol* **57**, 543-556 (2011).

40 Scherler, D., Bookhagen, B. & Strecker, M. R. Hillslope-glacier coupling: The interplay of topography and glacial dynamics in High Asia. *J. Geophys. Res.-Earth* **116** (2011).

41 Abdallah, H., Bailly, J. S., Baghdadi, N. & Lemarquand, N. Improving the assessment of ICESat water altimetry accuracy accounting for autocorrelation. *ISPRS J. Photogramm.* **66**, 833-844 (2011).

42 Kääb, A. Glacier volume changes using ASTER satellite stereo and ICESat GLAS laser altimetry. A test study on Edgeoya, eastern Svalbard. *IEEE T. Geosci. Remote* **46**, 2823-2830 (2008).

43 Fricker, H. A. *et al.* Assessment of ICESat performance at the Salar de Uyuni, Bolivia. *Geophys. Res. Lett.* **32** (2005).

44 Carabajal, C. C. & Harding, D. J. SRTM C-band and ICESat laser altimetry elevation comparisons as a function of tree cover and relief. *Photogramm. Eng. Rem. S.* **72**, 287-298 (2006).

45 Schutz, B., DiMarzio, J., Luthcke, S., Hancock, D. & Urban, T. Notice concerning detection of ICESat/GLAS inter-campaign elevation biases. (NSIDC, 2011).

46 Shuman, C. A., Harding, D. J., Cornejo, H. G. & Suchdeo, V. P. in *2010 Fall Meeting, AGU* C41A-0491 (San Francisco, 2010).

47 Rodriguez, E., Morris, C. S. & Belz, J. E. A global assessment of the SRTM performance. *Photogramm. Eng. Rem. S.* **72**, 249-260 (2006).

48 Rignot, E., Rivera, A. & Casassa, G. Contribution of the Patagonia Icefields of South America to sea level rise. *Science* **302**, 434-437 (2003).

49 Paul, F. & Haeberli, W. Spatial variability of glacier elevation changes in the Swiss Alps obtained from two digital elevation models. *Geophys. Res. Lett.* **35**, L21502 (2008).

50 Schiefer, E., Menounos, B. & Wheate, R. Recent volume loss of British Columbian glaciers, Canada. *Geophys. Res. Lett.* **34** (2007).

51 Larsen, C. F., Motyka, R. J., Arendt, A. A., Echelmeyer, K. A. & Geissler, P. E. Glacier changes in southeast Alaska and northwest British Columbia and contribution to sea level rise. *J. Geophys. Res.-Earth* **112** (2007).

52 Müller, K. *Microwave penetration in polar snow and ice: implications for GPR and SAR*. Vol. 1090 (Faculty of Mathematics and Natural Sciences. University of Oslo, 2011).

53 Dall, J., Madsen, S. N., Keller, K. & Forsberg, R. Topography and penetration of the Greenland ice sheet measured with airborne SAR interferometry. *Geophys. Res. Lett.* **28**, 1703-1706 (2001).

54 Berthier, E., Arnaud, Y., Vincent, C. & Remy, F. Biases of SRTM in high-mountain areas: Implications for the monitoring of glacier volume changes. *Geophys. Res. Lett.* **33**, L08502 (2006).

55 Möller, M. & Schneider, C. Volume change at Gran Campo Nevado, Patagonia, 1984-2000: a reassessment based on new findings. *J. Glaciol.* **56**, 363-365 (2010).

56 Burbank, D. W. *et al.* Bedrock incision, rock uplift and threshold hillslopes in the northwestern Himalayas. *Nature* **379**, 505-510 (1996).

57 Vance, D., Bickle, M., Ivy-Ochs, S. & Kubik, P. W. Erosion and exhumation in the Himalaya from cosmogenic isotope inventories of river sediments. *Earth. Planet. Sc. Lett.* **206**, 273-288 (2003).

58 Boulton, G. S. in *Glacial Geomorphology* (ed D.R. Coates) 47-87 (State University of New York, 1974).

59 Hallet, B., Hunter, L. & Bogen, J. Rates of erosion and sediment evacuation by glaciers: A review of field data and their implications. *Global Planet. Change* **12**, 213-235 (1996).

60 Benn, D. I. & Evans, D. J. A. *Glaciers and glaciations*. (Arnold, 1998).

61 Bahr, D. B. & Radic, V. Significant total mass contained in small glaciers. *Cryosphere Discuss.* **6**, 737-757 (2012).

62 Cogley, J. G. Present and future states of Himalaya and Karakoram glaciers. *Ann. Glaciol.* **52**, 69-73 (2011).

63 Bader, H. Sorge's law of densification of snow on high polar glaciers. *J. Glaciol.* **2**, 319-323 (1954).

64 Hagg, W. J., Braun, L. N., Uvarov, V. N. & Makarevich, K. G. A comparison of three methods of mass-balance determination in the Tuyuksu glacier region, Tien Shan, Central Asia. *J. Glaciol.* **50**, 505-510 (2004).

65 Sapiano, J. J., Harrison, W. D. & Echelmeyer, K. A. Elevation, volume and terminus changes of nine glaciers in North America. *J. Glaciol.* **44**, 119-135 (1998).

66 Krimmel, R. M. Analysis of difference between direct and geodetic mass balance measurements at South Cascade Glacier, Washington. *Geogr. Ann. A.* **81A**, 653-658 (1999).

67 Thibert, E., Blanc, R., Vincent, C. & Eckert, N. Glaciological and volumetric mass-balance measurements: error analysis over 51 years for Glacier de Sarennes, French Alps. *J. Glaciol.* **54**, 522-532 (2008).

68 Copland, L. *et al.* Expanded and recently increased glacier surging in the Karakoram. *Arct. Antarct. Alp. Res.* **43**, 503-516 (2011).

69 Heid, T. & Kääb, A. Repeat optical satellite images reveal widespread and long term decrease in land-terminating glacier speeds. *Cryosphere* **6**, 467-478 (2012).

70 Vincent, C. *et al.* Ice ablation as evidence of climate change in the Alps over the 20th century. *J. Geophys. Res.-Atmos.* **109**, D10104 (2004).

71 Barrand, N. E., Murray, T., James, T. D., Barr, S. L. & Mills, J. P. Optimizing photogrammetric DEMs for glacier volume change assessment using laser-scanning derived ground-control points. *J. Glaciol.* **55**, 106-116 (2009).

72 Jokinen, O. in *Remote Sensing of Glaciers* (eds P. Pellikka & G. Rees) 245-268 (CRC Press/Balkema, 2010).

73 Lang, S. *et al.* Assessing components of the natural environment of the Upper Danube and Upper Brahmaputra river basins. *Adv. Sci. Res.* **7**, 21-36 (2011).

74 Treydte, K. S. *et al.* The twentieth century was the wettest period in northern Pakistan over the past millennium. *Nature* **440**, 1179-1182 (2006).

75 Quincey, D. J. *et al.* Karakoram glacier surge dynamics. *Geophys. Res. Lett.* **38**, L18504 (2011).

76 Quincey, D. J. *et al.* Ice velocity and climate variations for Baltoro Glacier, Pakistan. *J. Glaciol.* **55**, 1061-1071 (2009).

77 Xu, B. Q. *et al.* Black soot and the survival of Tibetan glaciers. *P Natl Acad Sci USA* **106**, 22114-22118 (2009).

78 Oerlemans, J., Giesen, R. H. & Van den Broeke, M. R. Retreating alpine glaciers: increased melt rates due to accumulation of dust (Vadret da Morteratsch, Switzerland). *J. Glaciol.* **55**, 729-736 (2009).